Sexton-Oates *et al. Molecular Cancer* (2026) 25:204
https://doi.org/10.1186/s12943-026-02721-7

Molecular Cancer

RESEARCH Open Access

Deep molecular profiling of lung neuroendocrine tumours and supra-carcinoids

Alexandra Sexton-Oates[1†], Émilie Mathian[1†], Noah Candeli[2], Yuliya Lim[1], Catherine Voegele[1], Alex Di Genova[3,4,5], Laurane Mangé[1], Zhaozhi Li[6], Tijmen van Weert[7], Lipika Kalson[1,8], Tiffany M. Delhomme[1], Lisa M. Hillen[7], Ricardo Blázquez-Encinas[9,10,11], Abel Gonzalez-Perez[12,13,14], Maike L. Morrison[15,16], Eleonora Lauricella[17], Lise Mangiante[1,18], Lisa Bonheme[1], Laura Moonen[7], Gudrun Absenger[19], Janine Altmuller[20,21], Cyril Degletagne[22], Odd Terje Brustugun[23,24,25], Vincent Cahais[26], Giovanni Centonze[27], Amélie Chabrier[1], Cyrille Cuenin[26], Francesca Damiola[28], Vincent Thomas de Montpréville[29], Jean-François Deleuze[30], Anne-Marie C. Dingemans[31], Élie Fadel[29,32], Nicolas Gadot[28], Akram Ghantous[26], Paolo Graziano[33,34], Paul Hofman[35], Véronique Hofman[35], Alejandro Ibáñez-Costa[9,10,11], Stéphanie Lacomme[36], Nuria Lopez-Bigas[12,13,14,37], Marius Lund-Iversen[38], Massimo Milione[27], Lucia Anna Muscarella[39], Sergio Pedraza-Arevalo[9,10,11], Corinne Perrin[40], Gaetane Planchard[41], Helmut Popper[42], Luca Roz[43], Angelo Sparaneo[39], Wieneke Buikhuisen[44], José van den Berg[45], Margot Tesselaar[46], Jaehee Kim[6], Ernst Jan M. Speel[47], Séverine Tabone-Eglinger[48], Thomas Walter[49,50], Gavin M. Wright[51,52], Justo P. Castaño[9,10,11,53], Lara Chalabreysse[54], Liming Chen[55,56], Christophe Caux[57], Marco Volante[58], Nicolas Girard[59,60,61], Jean-Michel Vignaud[62], Esther Conde[63,64], Audrey Mansuet-Lupo[65], Luka Brcic[66,67], Giuseppe Pelosi[68], Mauro Giulio Papotti[69], Sylvie Lantuejoul[70,71], Jules Derks[31], Talya Dayton[2], Nicolas Alcala[1*†], Matthieu Foll[1*] and Lynnette Fernandez-Cuesta[1*]

[†]Alexandra Sexton-Oates, Émilie Mathian and Nicolas Alcala contributed equally to this work.

*Correspondence:
Nicolas Alcala
alcalan@iarc.who.int
Matthieu Foll
follm@iarc.who.int
Lynnette Fernandez-Cuesta
fernandezcuestal@iarc.who.int

Full list of author information is available at the end of the article

Abstract

Background Lung neuroendocrine tumours (NETs, also known as carcinoids) are rapidly rising in incidence worldwide but have unknown aetiology and limited therapeutic options beyond surgery. The current WHO classification, based on mitotic count and presence or absence of necrosis, divides lung NETs into grade-1 typical, and grade-2 atypical tumours. This dichotomous classification however does not account for recently described molecular entities nor is it sufficient for clinical management.

Methods Here we conducted integrative multi-omic analyses on over 300 lung NETs including whole-genome sequencing, transcriptome profiling, and DNA methylation arrays, followed by archetype analysis, to identify and characterise molecular groups. We further investigated molecular groups using spatial RNA sequencing and proteomics, and deep learning analysis of whole slide images.

Results The integration of multi-omic data provided definitive proof of the existence of four strikingly different molecular groups that vary in patient characteristics, genomic and transcriptomic profiles, microenvironment, and morphology. Among these, we identified a new molecular group, enriched for highly aggressive supra-carcinoids that displayed an immune-rich microenvironment linked to tumour-macrophage crosstalk. We uncovered an undifferentiated cell population within supra-carcinoids and show the transcriptomic similarities between supra-carcinoids and the recently identified atypical small cell lung cancer tumours, further demonstrating their molecular link to high-grade lung neuroendocrine carcinomas. Multi-regional genomic analyses identified distinct evolutionary trajectories, suggesting that molecular groups are determined early in tumourigenesis by genomic events, and that transitions between groups, though infrequent, are possible for supra-carcinoids. Deep learning models accurately identified these groups based on morphology alone, outperforming current histological criteria. Together with the validation of a panel of immunohistochemistry markers, we demonstrated that these molecular groups can be accurately identified based on morphological features, facilitating their future implementation in the clinical setting. Our proposed morpho-molecular classification highlights potential group-specific therapeutic opportunities, with differences in expression to DLL3, EGFR, FGFR and TERT inhibitor targets.

Conclusions Overall, our findings unify previously proposed molecular classifications and refine the lung cancer map by revealing novel tumour phenotypes with potential implications for prognosis and therapeutic management.

Keywords Cancer, Pulmonary carcinoids, Genomics, Multi-omics, Deep-learning

Background

Lung neuroendocrine tumours (NETs, also known as carcinoids) and neuroendocrine carcinomas (NECs, including small-cell lung cancer, SCLC, and large-cell neuroendocrine carcinoma, LCNEC) are considered to be distinct diseases due to their differing aetiologies and clinical behaviour, with NECs being much more aggressive and strongly linked to smoking, unlike NETs [1, 2]. According to the World Health Organisation (WHO) Classification of Thoracic Tumours, mitotic count and necrosis differentiate grade-1 typical from grade-2 atypical tumours, with five-year overall survival rates of 90% and 60%, respectively [1, 3]. However, the current morphological classification has limited predictive value for treatment response, and its prognostic value is hindered by significant inter-observer variability [4, 5]. We previously identified three distinct transcriptomic groups of lung NETs (Ca A1, Ca A2, and Ca B [6, 7]) each comprising a mixture of grade-1 and grade-2 tumours, which have been validated in independent studies and are starting to guide clinical research [8–12]. However, the misalignment between the morphological and molecular classifications and their respective biological relevance poses a dilemma for their implementation in clinical practice [13, 14]. Previously we also reported six cases of a new entity, named "supra-carcinoid", with low-grade morphology but molecular and clinical features resembling those of SCLC and LCNEC [6], and suggested that this new biological entity might be responsible for the poor prognosis observed in a subset of lung NETs [15]. The discovery of supra-carcinoids further questions the assumption that lung NETs and NECs are unrelated diseases [16]. However, the limited number of samples and molecular data generated has hindered the identification of diagnostic or targetable features of this aggressive group, as well as the investigation of the molecular mechanisms and evolutionary trajectories leading to each group.

In the current study, we leverage a unique series of 319 fresh frozen lung NETs, including matched normal material, enriched for the more aggressive grade-2 tumours ($n = 79$), coupled with detailed histopathological annotations and whole-slide images, primarily sourced from the lungNENomics network [5]. On this series, we have performed multi-omic analyses and state-of-the-art spatial omics and deep learning analyses to better understand supra-carcinoid biology, the development of lung NET

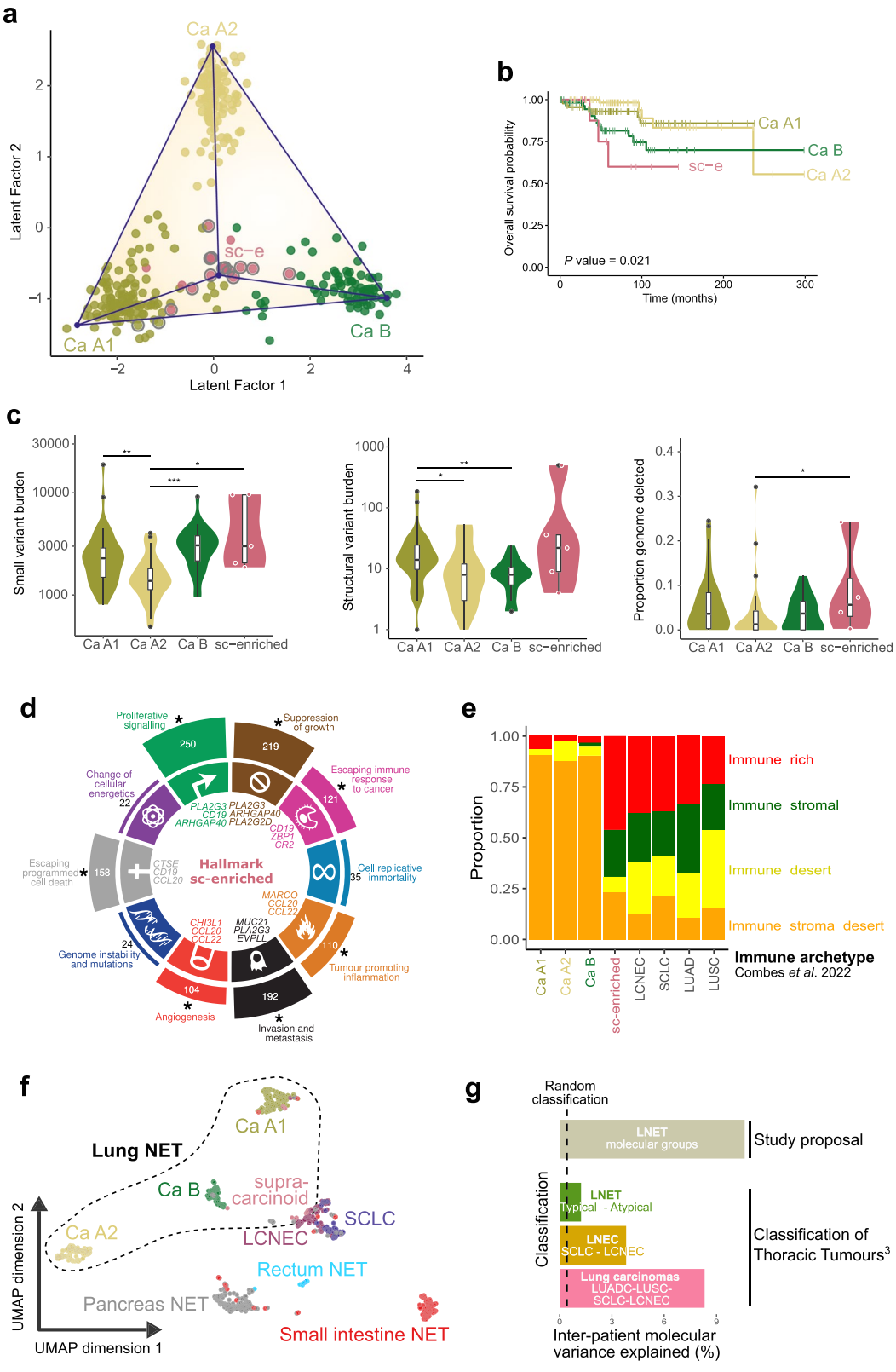

Fig. 1 (See legend on next page.)

(See figure on previous page.)

Fig. 1 Supra-carcinoids constitute the fourth distinct molecular group of lung NETs. **a** 319 tumours from the lung neuroendocrine tumour (NET) cohort plotted over MOFA Latent Factors 1 and 2, contained within a tetrahedron (blue lines) formed by four phenotypic archetypes (blue dots) identified through ParetoTI. Archetype positions are labelled by molecular group, and tumours are coloured by molecular group membership ($n = 121$ Ca A1, $n = 107$ Ca A2, $n = 75$ Ca B, $n = 16$ sc-enriched). Supra-carcinoids are circled in grey ($n = 16$). sc-e, supra-carcinoid enriched. **b** Kaplan–Meier plot of overall survival probability over time in months per molecular group (P value = 0.021, Log-rank test). **c** Violin plot of the distribution of the small variant burden (left), structural variant burden (centre), and proportion of genome deleted (right) in the lung NET cohort (y-axis) as a function of the molecular group classification (x-axis). Displays samples ($n = 102$) for which WGS data are available. Significance levels correspond to t-tests. * $0.01 < P$ value < 0.05; ** $0.001 < P$ value ≤ 0.01; *** P value ≤ 0.001. **d** Polar bar plot of the number of sc-enriched core upregulated genes per hallmark of cancer. Asterisks indicate that the corresponding hallmark is significantly enriched in sc-enriched core upregulated genes. The three genes per hallmark with the largest fold change in sc-enriched are displayed. **e** Proportion of samples assigned to four immune archetypes (y-axis) per molecular group or tumour type (x-axis). LCNEC, large cell neuroendocrine carcinoma; SCLC, small cell lung cancer; LUADC, lung adenocarcinoma; LUSC, lung squamous cell carcinoma, LNEC, lung neuroendocrine carcinoma. **f** Uniform Manifold Approximation and Projection (UMAP) of transcriptomes of neuroendocrine neoplasms from multiple organs ($n = 641$). NET, neuroendocrine tumour. **g** Proportion of variance in gene expression explained by the proposed and existing thoracic tumour classifications, where 0% indicates the classification explains no difference in gene expression profiles between patients and 100% indicates that all differences between patients are explained by the classification. The dashed line corresponds to the value expected under a random classification, obtained using permutations of the molecular group labels

molecular groups, and the relationship between NETs and NECs. We further aimed to propose a unified morpho-molecular classification of lung NETs to ultimately improve diagnosis and clinical management.

Methods

See attached document entitled (Supplementary Material 1: Supplementary Methods).

Results

Beyond anecdotal case reports, supra-carcinoids constitute the fourth distinct molecular group of lung NETs

We conducted Multi-Omics Factor Analysis (MOFA [17]) incorporating gene expression ($n = 273$), DNA methylation ($n = 247$), small and structural variant, and copy number variant data ($n = 102$) on a cohort of 319 lung NETs [18] (Supplementary Figs. S1, S2a-d, Supplementary Tables S1-S3). Archetype analysis (ParetoTI [19, 20]) was applied to the resulting factors of variation and demonstrated the existence of four distinct molecular archetypes, three of which aligned with our previously identified molecular groups (Ca A1, Ca A2, and Ca B [6]). The fourth archetype was enriched for supra-carcinoid [6, 7] (14 of 16 tumours) and is hereafter referred to as sc-enriched (Fig. 1a, Supplementary Fig. S2e-h, Supplementary Tables S1, S4-S5). A mixture of grade-1 and grade-2 NETs were found in each molecular group, however Ca B and sc-enriched contained a higher proportion of grade-2 tumours than Ca A1 and Ca A2 (33% and 63%, versus 21% and 18%, respectively). Unlike the other molecular groups, sc-enriched tumours displayed no propensity for any particular sex, age, or location, but were significantly more likely to display pleural invasion, and had poorer overall survival, including when adjusted for sex and stage (Fig. 1b, Table 1, Supplementary Tables S5-S7).

Genomically, sc-enriched had higher mutational, structural variant and deletion burdens compared to other groups (Fig. 1c, Supplementary Table S8). Accordingly, signature variability analysis [21] showed that sc-enriched tumours displayed significantly more diverse mutational repertoires, suggesting that they undergo more mutational processes than tumours from other groups (Supplementary Fig. S3, Supplementary Table S9). Additionally, sc-enriched tumours showed significantly more hallmarks of cancer [22, 23] impacted by small variants than the other three groups (cell replicative immortality, escaping immune response to cancer, and proliferative signalling) (Supplementary Fig. S4, Supplementary Table S10). Similar results were obtained from transcriptomic data where it was found that the sc-enriched samples had the greatest number of core upregulated genes, and that, contrary to the other molecular groups, these genes were enriched for hallmarks of cancer (seven out of ten), including escaping immune response to cancer, and proliferative signalling (Fig. 1d, Supplementary Tables S1, S11-S12). In line with this, sc-enriched tumours had a significantly higher proliferation index [24, 25], even when considering grade-2 tumours only (Supplementary Table S13).

Cell deconvolution of transcriptomic data [26, 27] demonstrated that the sc-enriched group had significantly higher immune infiltration (dominated by classically activated M1 macrophages [26, 28]), and cancer associated fibroblast (CAF) levels than other lung NET groups, aligning it with recently proposed immune- and stromal-rich tumour immune archetypes [29, 30], contrary to Ca A1, Ca A2, and Ca B that were predominantly classed as immune-desert archetypes (Fig. 1e, Supplementary Fig. S5, Supplementary Tables S14-S16). Moreover, most of the sc-enriched core upregulated genes were associated with the immune system, including a high proportion of chemokine ligand genes, with 56% linked to regulation of immune system process, leukocyte migration, or regulation of humoral immune response (Supplementary Table S17). These findings establish supra-carcinoids as a distinct and robust molecular group of lung NETs, with a more clinically and molecularly aggressive profile, associated with a unique tumour microenvironment.

Table 1 Main features of supra-carcinoids ($n = 16$)

Morphological features	Histological type	2 typical, 11 atypical, 2 carcinoid, 1 NET G3
	Mean mitotic count	5.5
	Mean % of ki-67	15%
	Pleural invasion	4 (out of 6 tumours)
Clinical and epidemiological features	10-year overall survival rate	47%
	Sex	8 female, 8 male
	Stage	3 IA, 3 IB, 1 IIA, 2 IIB, 1 IIIA, 1 IIIB, 1 IIIC, 1 IV, 3 unknown
	Asbestos exposure	2 (out of 3)
	Smoking	4 never, 2 former, 3 current, 7 unknown
Molecular features	*MEN1* damaging mutations	2 (out of 5)
	BRAF V600E	2 (out of 5)
	TERT overexpression	8 (out of 12)
	Diverse mutational repertoire	Three hallmarks of cancer affected
	1330 core upregulated genes*	Seven hallmarks of cancer affected
Tumour microenvironment features		Mostly linked with the immune system
	Immune infiltration	30% (quanTIseq estimate)
	Levels of cancer associated fibroblasts	4% (EPIC estimate)

*Analysis performed with supra-carcinoid enriched molecular group, therefore included all supra-carcinoid with RNA-seq data ($n = 12$) and one non supra-carcinoid (LNET16T)

Dimension-reduction analysis of transcriptomic data from lung, pancreatic, small intestine, and rectal neuroendocrine neoplasms (NENs) [31–33] revealed that only lung NETs formed distinct clusters, and all other neoplasms clustered homogenously by their organ of origin (Fig. 1f). Whilst molecular groups of digestive NETs have been identified [34], these findings indicate that within the family of NENs, lung NET molecular groups are uniquely distinct from one another. As a measure of molecular group distinctiveness, and how well the four-group categorisation captures differences between lung NET patients in comparison to the existing classification, we calculated the percentage of molecular variation explained by the current classifications. We found that the four groups explain more inter-patient molecular variance than the WHO Classification of Thoracic Tumours [1], be that of lung NETs, lung NECs, or even that of all lung carcinomas (Fig. 1g). The existence of four distinct lung NET molecular groups suggests varied carcinogenesis processes; we thus set out to understand their origin and temporal evolution.

Ca A1, A2, and B are spatially stable and follow distinct evolutionary trajectories while supra-carcinoids may evolve from other groups

To assess whether the groups contained different cell states [35], hinting at different precursor cells or varied cell differentiation trajectories. We compared lung NET bulk expression profiles with a panel of single-cell sequencing reference profiles comprising epithelial cells from foetal lung tissue airway organoids, enriched for both lower airway progenitor (LAP) and pulmonary neuroendocrine cells, as well as lung NET microenvironment cells (stromal and immune) [36–38]. Deconvolution revealed that most tumours contained a mix of the terminally differentiated neuroendocrine cell types (CALCA +, NEUROD1 +), and club cells, however proportions did vary within and between molecular groups. Ca A1 had the highest proportion of differentiated neuroendocrine cells, while Ca B contained the highest proportion of club cells, and Ca A2 displayed a mixed profile of both cell types. The pulmonary neuroendocrine precursor, LAPs [38], were found in the highest proportion in sc-enriched samples and were virtually absent in Ca A1, Ca A2 and Ca B. Furthermore, sc-enriched tumours had similar proportions of LAP and differentiated neuroendocrine cells to LCNEC (Fig. 2a, Supplementary Fig. 6a, Supplementary Tables S14 & S18). Spatial transcriptomic analysis of four supra-carcinoids showed that these cell types occupy distinct spatial locations, with clear separation between CALCA + /NEUROD1 + areas and LAP areas (Fig. 2b, Supplementary Fig. S6b & S7, Supplementary Table S19).

We then explored the role of the tumour microenvironment in driving supra-carcinoid development. Spatial transcriptomics data confirmed that sc-enriched regions had specific microenvironments, co-localising with macrophages and fibroblasts (Fig. 2b, Supplementary Figs. S6b & S7, Supplementary Table S19). Cell–cell interaction inference [39] identified MIF (macrophage migration inhibitory factor) and collagen signalling pathways (commonly associated with fibroblasts) among the top-scored interactions present in the four supra-carcinoid samples, and importantly, key genes involved in these pathways, *CD44* and *CD74* (MIF), and *COL1A1* and *COL1A2* (collagen), were found to be spatially correlated with sc-enriched regions (Supplementary Fig. S8, Supplementary Table S20).

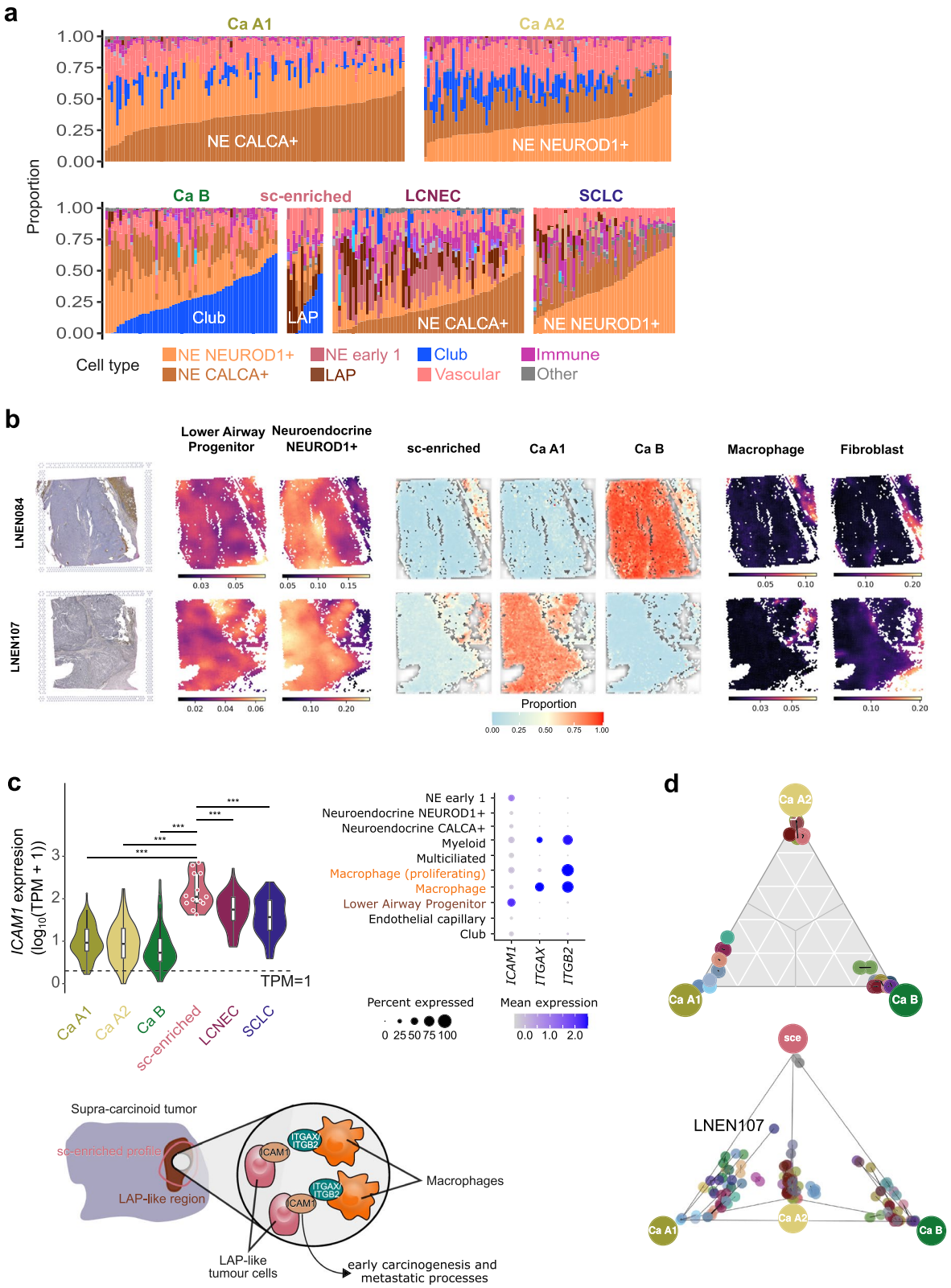

Fig. 2 (See legend on next page.)

(See figure on previous page.)

Fig. 2 Supra-carcinoids harbour a unique cell state and microenvironment. **a** Estimated proportion (y-axis) of cell types per sample (x-axis), using deconvolution with a custom single-cell reference database including a diverse repertoire of neuroendocrine cells. NE: neuroendocrine; LAP, lower airway progenitor. Displays samples from the lung NETcohort ($n = 273$), LCNEC ($n = 69$), and SCLC ($n = 51$) for which RNA-seq data are available. **b** Spatial transcriptomic images of two supra-carcinoid samples. From left to right, columns represent: the H&E image, proportion of lower airway progenitor cell expression profile per spot, proportion of neuroendocrine NEUROD1 + cell expression profile per spot, proportion of sc-enriched group expression profile per spot, proportion of CA A1 group expression profile per spot, proportion of Ca B group expression profile per spot, and the estimated location and proportions of macrophages and fibroblasts (scaled so 1 is the maximal value observed in a given sample). **c** Distribution of *ICAM1* expression by molecular group, TPM, transcripts per kilobase million, asterisks correspond to significance assessed by t-tests (left), mean expression (scaled read counts) of genes *ICAM1*, *ITGBX*, and *ITGB2* obtained from single-cell data for cell types present within sc-enriched samples (right, from panel **a**), and schematic of interaction between LAP-like cells, macrophages, ICAM-1 and the ITGBX/ITGB2 heterodimer (bottom). * $0.01 < P$ value < 0.05; ** $0.001 < P$ value ≤ 0.01; *** P value ≤ 0.001. **d** Ternary plots depicting the relative position of intra-tumoural heterogeneity (ITH) samples in space between different molecular groups. Black lines join ITH samples from the same patients. ITH samples are coloured by patient. Patient LNEN107 highlighted as the patient whose ITH samples were assigned to two different molecular groups

Furthermore, a significant cell–cell interaction involving sc-enriched regions was detected between the LAP marker *ICAM1*, whose expression is highly specific to sc-enriched tumours, and two macrophage markers, *ITGAX* and *ITGB2* (Fig. 2c, Supplementary Fig. S8b-c, Supplementary Tables S19-S20). The *ICAM1* pathway is known to be involved in wound healing, early carcinogenesis, and the metastatic process [40], hinting at the role of tumour-macrophage interactions in supra-carcinoids.

Spatial analysis also demonstrated that the supra-carcinoids contained regions with a molecular profile similar to that of the Ca A1 or Ca B groups, as well as sc-enriched (Fig. 2b, Supplementary Fig. S6c). We found that the sc-enriched profile was significantly spatially correlated with the LAP cell profile, while the Ca A1 and Ca B profiles were significantly spatially correlated with CALCA + and NEUROD1 + cell profiles (Supplementary Figs. S6c & S7, Supplementary Table S19). To examine the possibility that supra-carcinoids may arise from other molecular groups, we performed multi-region multi-omics integration of 90 tumour samples from 41 patients. Subsequent archetype analysis demonstrated that in 40/41 patients, all tumour regions belonged to the same molecular group, and that the only tumour that had regions belonging to different groups (Ca A1 and sc-enriched) was a supra-carcinoid (LNEN107, Fig. 2d, Supplementary Fig. S9a, Supplementary Table S21). Visualisation of the multi-regional samples within the latent factor space demonstrated that tumour regions differed in location primarily across the axes separating sc-enriched from the other three molecular groups (Fig. 2d, Supplementary Fig. S9b). This suggests that groups are generally spatially stable, but that transitions between groups, though infrequent, are possible for supra-carcinoids.

To further explore molecular group development, we examined genomic driver alterations [41, 42] and evolutionary trajectories. Eight significantly recurrent copy number variant (CNV) events were identified as drivers at the cohort level, and an additional three at the level of individual molecular groups. These were amplifications of *chr 4* (Ca B-driver), *chr 5* (encompassing *TERT*), *chr 7, chr 8* (Ca A2), and *chr 14p* (cohort-level and Ca A1), and deletions of *chr 1p13.3*, *chr 3* (cohort-level and Ca A1), *chr 11q13.1* (encompassing *MEN1*), and *chr 11* (Ca B) (Fig. 3a-b, Supplementary Tables S22-S24). Whilst sc-enriched did harbour driver CNVs, none were specifically enriched within the group (Fig. 3a-b). Most driver mutations were clonal and almost exclusive to a single molecular group, including *EIF1AX* (only in Ca A1, $n = 6$), *BRAF* (V600E, only in sc-enriched, $n = 2$), *MEN1* (9/11 in Ca B), and *ARID1A* (4/6 clonal mutations in Ca A2), suggesting that molecular groups are determined early by genomic events (Supplementary Fig. S9c, Supplementary Tables S25-S29). This was further corroborated by phylogenetic analyses [43], identifying 26 significant driver-to-driver (small variant and CNV) trajectories (Fig. 3c, Supplementary Fig. S9d, Supplementary Table S30). These analyses showed that alterations associated with the molecular groups were predominantly initiation events, while alterations shared across groups were typically subsequent events (Fig. 3c). In contrast, sc-enriched emerged through multiple trajectories which were common to other groups and were more likely to have undergone secondary driver events, further suggesting that they may have evolved from other entities (Fig. 3b-c).

Supra-carcinoids may represent an intermediate step between NETs and NECs

In terms of lung NEN development, a question remains whether supra-carcinoids may represent a transitional biological entity between lung NETs and NECs [44, 45]. In support of this proposition, we report here upon a supra-carcinoid patient for which a patient-derived tumour organoid (PDTO) was created [46]. LNET10, a 26-year-old female never-smoker, was diagnosed with an atypical carcinoid at stage IA (T1bN0M0), with two mitoses/2mm^2, focal necrosis, and Ki-67 index of 20%. Molecular analysis of both the primary tissue and PDTO passage 4 (p4) identified moderately high *MKI67* expression (5 and 14 TPM, respectively), *BRAF* (V600E) and *PTEN* mutations, expression-based clustering with

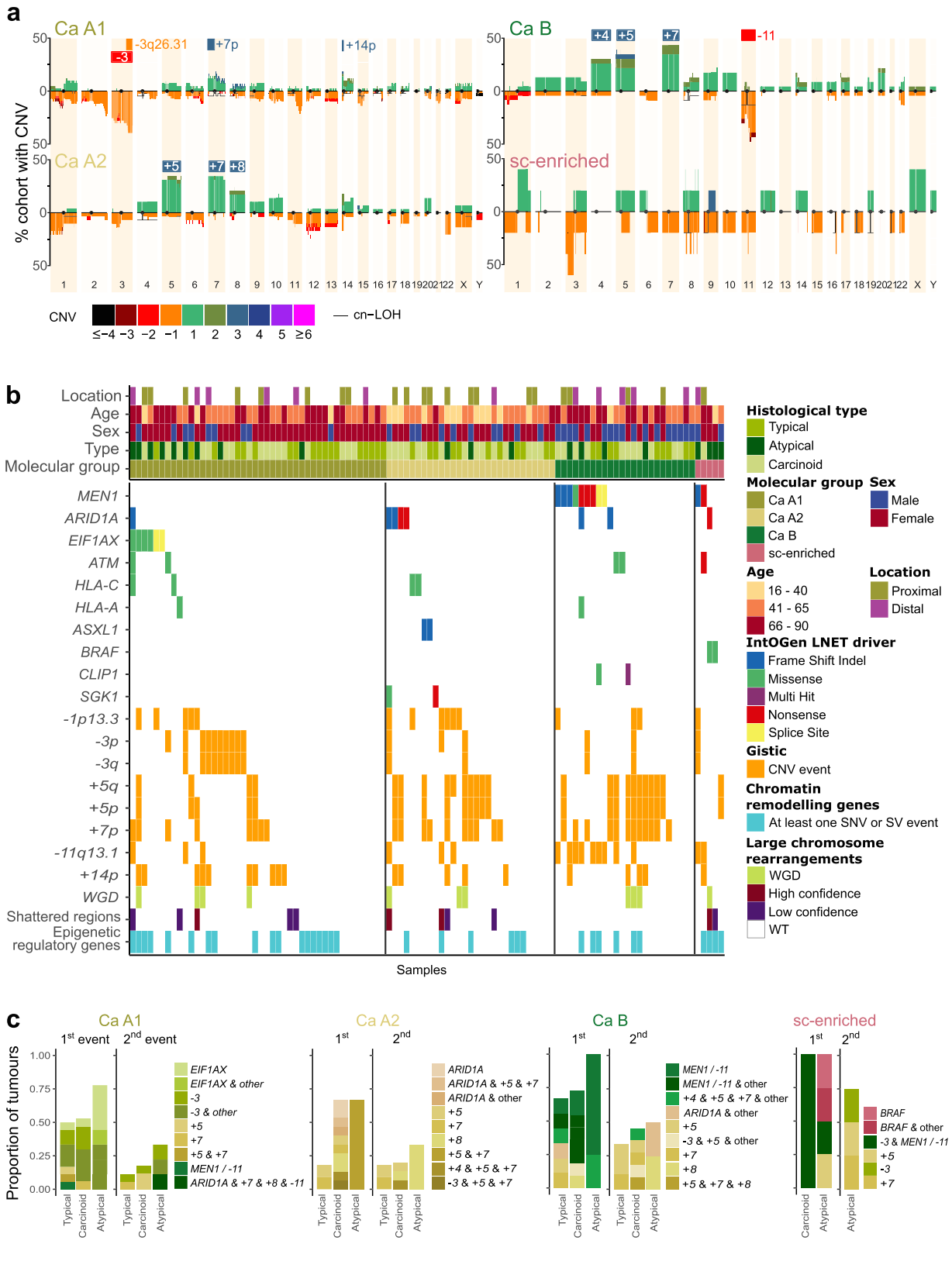

Fig. 3 (See legend on next page.)

(See figure on previous page.)

Fig. 3 Molecular groups are spatially stable and follow distinct evolutionary trajectories. **a** Copy number profile of each molecular group; the y-axis represents the percentage of samples in each group with a given alteration (amplifications above the 0 line, deletions below), and colours represent the copy number. The black line represents copy-neutral loss of heterozygosity (cn-LOH). Driver copy number variants (CNVs) detected in each group by the GISTIC2 method are represented by a square above each profile (red rectangles for deletions, blue rectangles for amplifications). **b** Oncoplot of small variants in IntOGen identified driver genes, CNV drivers identified by GISTIC2, and large chromosomal rearrangements. Selected clinical features and molecular group assignment are represented at the top along the x-axis. **c** Recurrent evolutionary trajectories based on small variants and CNV drivers detected using the REVOLVER method. Colours represent the driver event, "1st event" refers to initiating events (trajectories from germline to a driver in Supplementary Fig. S9d), and "2nd event" refers to subsequent events (trajectories between two drivers in Supplementary Fig. S9d). **a**-**c** Display samples from the lung NET cohort with WGS data ($n = 102$)

LCNEC [46], and a chromothripsis-like clustered structural variant pattern affecting *chr 9* (Fig. 4a, Supplementary Tables S1-S2, S25, S27-S28). One year after diagnosis, metastatic disease in the skin and lymph nodes was noted, and the patient was then treated with BRAF and MEK inhibitors, dabrafenib and trametinib, respectively. After an initial response, bone and liver metastases developed, and biopsy of the liver metastasis followed by whole-genome sequencing revealed a deletion in exons 2–8 of *BRAF*, a known mechanism of resistance to BRAF inhibitor therapy [47], that was absent in the p4 PDTO. Crucially, based on the liver biopsy, the pathologist revised the diagnosis to LCNEC, suggesting that a full transformation to NEC may have occurred (Fig. 4a). The LNET10 PDTO was one of the fastest-growing lung NET PDTOs, taking around three months to reach passage three versus on average six months for the others, and displayed an increase in mutational burden and *MKI67* gene expression over time, from the primary to passage 11 (p11), thus reflecting the tumour aggressiveness seen in the patient (Fig. 4a). We subsequently assessed the cell type make-up of the primary and PDTO passages and noted a shift from a NET-like to NEC-like profile over time, exemplified by the reduction in LAP and club cells, and increase in NE early 1 cells, between p4 and p11, despite the lack of microenvironment in culture (Fig. 4a, Supplementary Table S14).

Chromothripsis is an infrequent event in lung NETs [6, 48], however the findings above suggest it may be important in the potential transformation from lung NET to NEC. Supporting this hypothesis is the recent publication of a subset of metastatic SCLC tumours with chromothripsis but lacking *RB1* and *TP53* co-inactivation, labelled 'atypical SCLC', several of which originated from a primary lung NET [49]. We combined the available transcriptomic data for these atypical SCLC tumours, which included two primary and four metastatic tumours with chromothripsis (one of which had a carcinoid primary), and one primary tumour with carcinoid histology (with atypical SCLC metastasis), with that of our sc-enriched tumours as well as 36 SCLC from George et al. [50] (which included one *TP53* and *RB1* wild-type SCLC also with chromothripsis) to examine the relationship between them (Fig. 4b). Hierarchical consensus clustering demonstrated that all chromothripsis-carrying SCLC tumours (whether metastatic or primary), as well as the primary lung NET that gave rise to metastatic SCLC, had transcriptomic features more closely related to supra-carcinoid than to conventional SCLC, raising the possibility that they may represent distinct evolutionary stages of supra-carcinoids (Fig. 4b).

Similar to the already established grade-3 NETs described in other organs a new morphological entity of lung NETs with carcinoid morphology but higher mitotic counts and Ki-67 levels than expected for such grade-1/2 tumours has now been formally recognised [14, 16, 51–55]. To assess whether supra-carcinoids correspond to this grade-3 lung NET entity, current and proposed lung NET diagnostic criteria of mitotic count and ki-67 index were evaluated by six individual pathologists for a subset of the cohort ($n = 197$). Although sc-enriched had significantly higher *MKI67* gene expression levels than other groups (9.4 TPM versus 1.6), the proliferative activity estimated via Ki-67 protein expression showed only a moderate increasing trend (Supplementary Fig. 10a, Supplementary Tables S1 & S13). In terms of mitotic count, mean count was significantly higher in Ca B tumours than those in Ca A1 (1.47 versus 0.86, Supplementary Fig. 10a). Only one supra-carcinoid exceeded the expected mitotic count and Ki-67 thresholds for lung NET and was classified as NET grade-3 by consensus. Five additional lung NETs were annotated by at least one pathologist as having more than ten mitoses/2mm^2 (although mean did not exceed ten). Of these five, four were classified as grade-1 or 2, and one as grade-3 by consensus. These higher mitotic count tumours were found in Ca A2 ($n = 1$), sc-enriched ($n = 2$) and Ca B ($n = 3$) molecular groups. Three of the remaining 15 lung NETs in the sc-enriched were classified as grade-1, ten as grade-2, and two as carcinoid not otherwise specified (Supplementary Table S13). This data suggests that supra-carcinoids can be but are not always grade-3.

The molecular classification of lung NETs provides additional information about biology and development

Molecular group classification also provided additional information on tumour biology and development masked by histological types. Distinct epidemiological characteristics were identified, particularly for the three largest groups. Ca A1 was enriched for females, patients

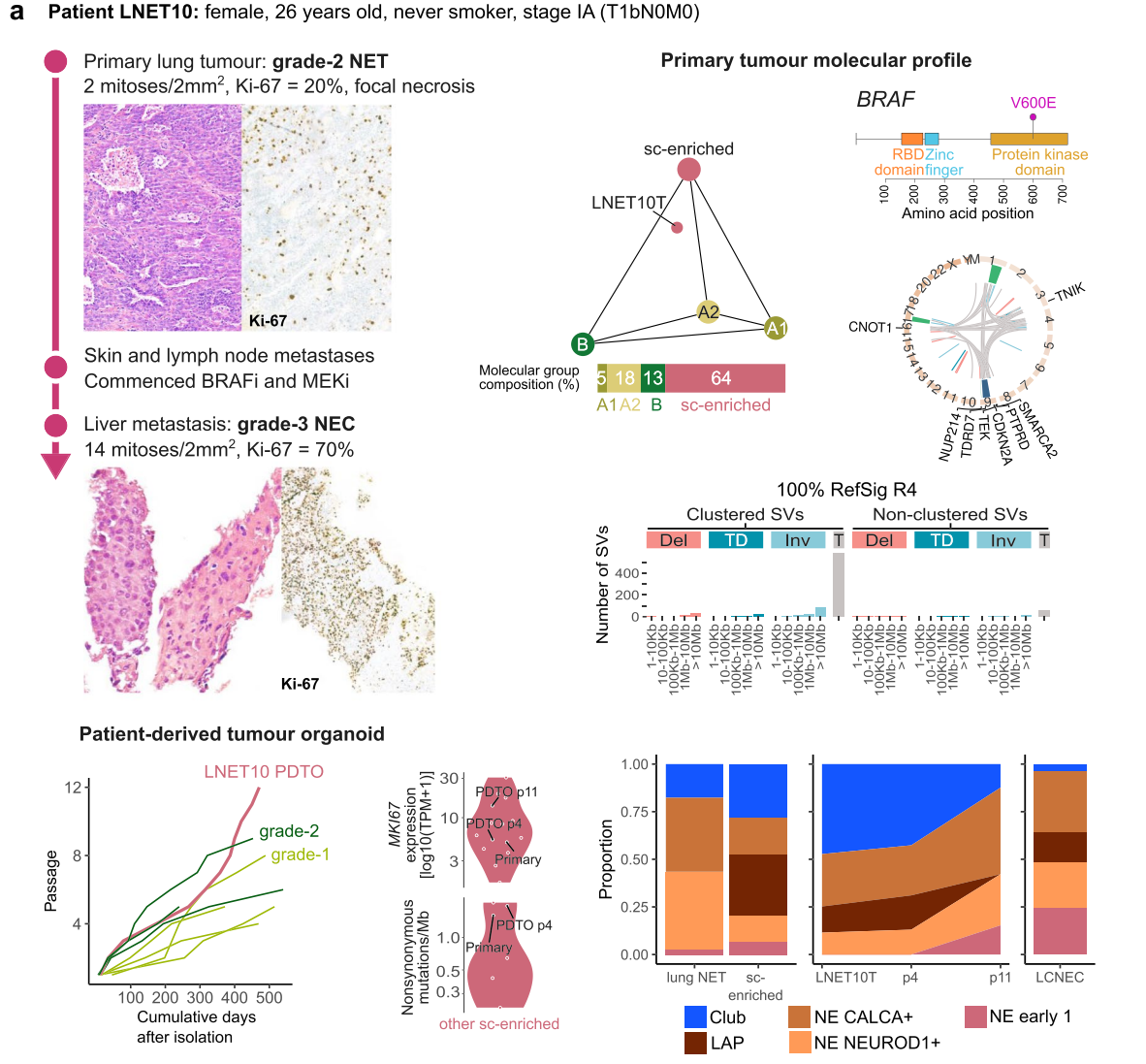

Fig. 4 (See legend on next page.)

(See figure on previous page.)

Fig. 4 Supra-carcinoids may represent an intermediate step between NETs and NECs. **a** Profile of a patient with a supra-carcinoid tumour for which a patient-derived tumour organoid (PDTO) was developed, allowing drug screens. Top left panel, clinical profile and disease course including H&E and Ki-67 stained pathology images. BRAFi, BRAF inhibitor; MEKi, MEK inhibitor; NET, neuroendocrine tumour; NEC, neuroendocrine carcinoma. Top right panel, molecular profile of primary tumour (LNET10T) showing location in archetype space (left), *BRAF* V600E alteration and shattered region of *chr9* (right), and structural variant (SV) signature profile of clustered translocations (T) corresponding to RefSig R4 (below). Del, deletions; TD, tandem duplications; Inv, inversions. Bottom panel, PDTO features of growth trajectory in comparison to other grade-1 and grade-2 lung NETs (left), *MKI67* expression and non-synonymous mutations per megabase (Mb) for primary tumour, PDTO passage 4 (p4) and passage 11 (p11) in comparison to other sc-enriched tumours (middle), and cell type proportions (right). Proportions for lung NET (Ca A1, Ca A2 and Ca B), sc-enriched and LCNEC are mean proportion per cell type for $n = 260$, $n = 13$, and $n = 69$ tumours, respectively. LAP, lower airway progenitor; NE, neuroendocrine. **b** Heatmap of differentially expressed genes between small cell lung cancer (SCLC) and supra-carcinoid enriched (sc-enriched) tumours with log fold change ≥ 2.5 ($n = 351$). Gene expression values for all samples ($n = 36$ SCLC, $n = 13$ sc-enriched, and $n = 7$ atypical SCLC) are plotted as log2(TPM + 1). Samples are arranged by consensus cluster order, and coloured bars indicate study of origin, sample origin, histology, presence of chromothripsis, smoking status, and entity

aged over 40, and distal locations. Similarly, Ca A2 was enriched for females but featured younger patients, comprising nearly all the under 40 cases, and were predominantly proximal tumours, whereas Ca B was enriched for males and patients over 40 (Fig. 5a, Supplementary Tables S1 & S5). Amongst grade-2 tumours only, smoking rates differed between molecular groups, whereby Ca B patients were significantly more often current or former smokers than Ca A2 (52% versus 11%, Fig. 5b, Supplementary Tables S1 & S5). Indeed, the smoking-associated ID3 mutational signature [56] was significantly more often present in Ca B than Ca A1 or Ca A2 (58%, 30%, and 24% of sequenced samples, respectively), and only within Ca B did tumours from ever smokers show stronger signs of clonal selection [57] than tumours from never smokers (Fig. 5b, Supplementary Fig. S3a-b, Supplementary Tables S8-S9). A significant difference in asbestos exposure was observed, albeit in low numbers of patients ($n = 1$ in Ca A1 and Ca A2, $n = 2$ in sc-enriched, and $n = 5$ in Ca B, Supplementary Tables S1 & S5). Furthermore, of 26 patients with a prior cancer diagnosis, 19 belonged to Ca A1; however, despite the associations with history of cancer in Ca A1, and young age at diagnosis in Ca A2, no recurrent germline variants were identified that clearly suggested underlying genetic susceptibility [58] (Supplementary Tables S1, S5, S31).

Group-specific core upregulated and downregulated genes showed that Ca A1 was the only molecular group to harbour enrichment for genes highly expressed in lung neuroendocrine cells [59], and in line with this, pathway analysis highlighted nervous system functions, and potential master transcription factors (TFs) for Ca A1 included proneural TFs *ASCL1* and *MYTL1* [60–62] (Fig. 5c, Supplementary Fig. S10b, Supplementary Tables S11, S17, S32-S33). *HNF4A* and *OTP* were identified as putative master TFs for Ca A2. Ca A2 and Ca B core upregulated genes both showed enrichment for the regulation of hormone levels pathway, and Ca B was associated with uronic acid metabolic process pathway (comprising the core upregulated *UGT* genes located on amplified *chr 4*, Fig. 5c, Supplementary Tables S11, S17, S33). Sc-enriched displayed the lowest expression of characteristic lung neuroendocrine cell genes [59] (Supplementary Fig. S10b, Supplementary Table S32).

Further analysis of transcriptomic data demonstrated that each molecular group had a dominant immune cell type: dendritic cells in Ca A1, alternatively activated (M2) macrophages in Ca A2, monocytes in Ca B, and classically activated (M1) macrophages [26, 28] in sc-enriched, though cell proportions varied within groups (Fig. 5d, Supplementary Tables S14-S15). Additionally, using digital spatial profiling the molecular groups Ca A1, Ca A2 and Ca B could be distinguished through the expression of immune-related proteins within tumoural and microenvironmental regions (Supplementary Fig. S10c-f, Supplementary Table S34).

Given the observation that molecular groups contain both grade-1 and 2 tumours (Fig. 5a), and the association between genomic instability and increased malignancy in cancer [23], we investigated genomic alteration burden by histological type. This analysis showed that in general grade-2 tumours harboured more genomic alterations than grade-1 tumours, suggesting that samples within each molecular group may have the potential to progress from grade-1 to 2 as part of their disease course, however this grade-effect was not always present within each molecular group (Figs. 3c & 5e, Supplementary Fig. S11, Supplementary Tables S1, S8, S10, S30).

Artificial intelligence and expert pathologists reveal morphological signatures of molecular groups

To identify whether there were morphological features specific to molecular groups that could assist in diagnosis, we used an agnostic approach of deep learning models [63, 64] followed by human interpretation of AI findings. Briefly, (i) whole slide images of HE/HES stained tumours were cut into small tiles, (ii) a deep learning model clustered the tiles into partitions which shared common morphological features, and (iii) the partitions were then annotated for morphological features by six expert pathologists (Supplementary Fig. S12a, Supplementary Tables S35-S40). Surprisingly, we found that the model performed better at predicting molecular groups

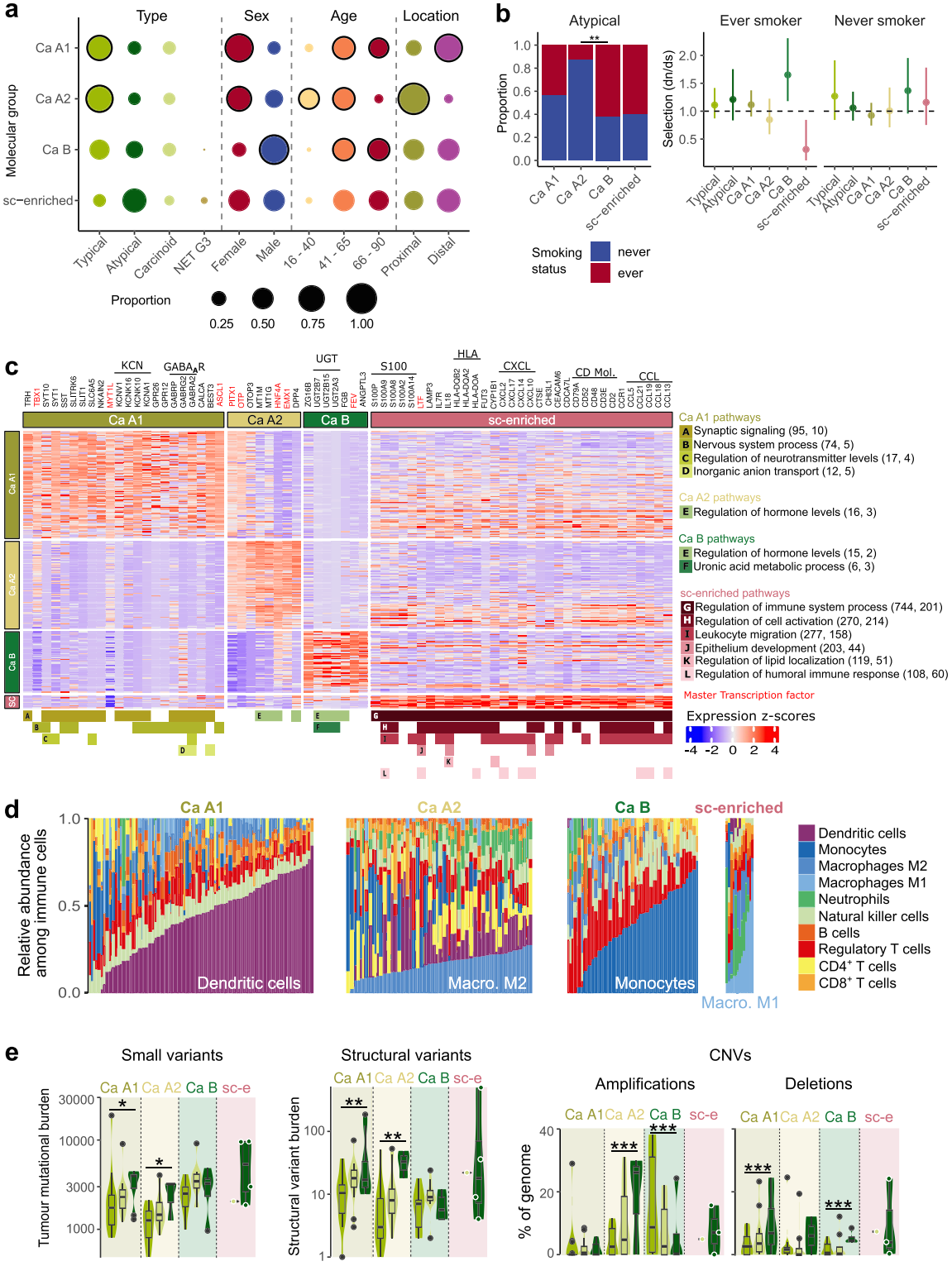

Fig. 5 (See legend on next page.)

(See figure on previous page.)

Fig. 5 Molecular groups provide complementary information to current classification. **a** Proportion per molecular group of each category within four feature groups: type (where "carcinoid" indicates tumours that could not be definitively classified as typical or atypical), sex (inferred from omics data), age category, and tumour location. Molecular group proportions per category within a feature group sum to 1. Circled features indicate significant enrichment within group (P value < 0.05, Binomial test). **b** Bar chart displaying the proportion of patients with grade-2 atypical lung NETs with and without a history of smoking (y-axis) per molecular group (x-axis), $n = 57$ for which data were available (left). Level of immunoediting, estimated as the selection coefficient of small variants in neoantigen-rich regions (ratio of non-synonymous to synonymous mutations, dN/dS) by the SOPRANO method within ever and never smoking patients, as a function of tumour type or molecular group (right). **c**, Expression heatmap of selected genes (columns) for each sample of the lung NET cohort (rows, $n = 273$). Gene expression values are displayed as z-scores of log2(TPM + 1) values. Genes are grouped by the molecular group for which they are either (i) a core upregulated gene and in a super-pathway (black), or (ii) a putative master transcription factor (red). Coloured bars on the bottom indicate gene membership in super-pathways, described in the legend on the right. Values between brackets next to the pathways correspond to the number of core upregulated genes (first value), and core pathways (second value), included in the super-pathway. **d** Relative abundance of ten immune cell types, in each molecular group, estimated from RNA-seq data using deconvolution (software quanTIseq). Individual samples are shown on the x-axis, relative abundances on the y-axis. **c**-**d** display lung NET cohort samples for which RNA-seq data are available ($n = 273$). **e** Distribution of genomic alteration burden within histological tumour types as a function of molecular group. Tumour types are ordered as follows: typical, carcinoid, atypical, colours are as per Fig. 5a. Stars represent the significance level of two-sided t-tests (small variants, structural variants), or permutation tests (copy number variations, CNVs). * $0.01 < P$ value < 0.05; ** $0.001 < P$ value ≤ 0.01; *** P value ≤ 0.001

(Ca A1, Ca A2, and Ca B, for which sufficient samples for analysis were available) than histological grades (Supplementary Fig. S12b-c). We found that Ca A1 tumour cells more frequently have a spindle shape, displayed nested cells, cells with clear cell changes, solid tissue architecture, and an enrichment for salt and pepper chromatin (Supplementary Figs. S12d, S13 & S14). Whilst Ca A1 and Ca A2 tumours shared an enrichment for fibrotic tissue, Ca A2 tumours more frequently had oncocytic changes, organoid tissue architecture, and plasmacytoid cells. Ca A2 and Ca B tumours also had more frequently an acinar tissue architecture than Ca A1 tumours. Tumour cell size was also found to be slightly different between the groups, with Ca A1 having marginally but significantly smaller cell sizes, and a smaller nucleus to cytoplasm ratio (Supplementary Figs. S12d, S13 & S14). Additional features were highly specific to certain partitions, such as cartilaginous tissue in partition 70, which was enriched for Ca A2 and Ca B (Supplementary Figs. S12d, S13 & S14). This finding is likely related to the more frequent proximal location of these tumours compared with Ca A1 and demonstrates the biological and clinical relevance of the model outputs. To test the generalisation of morphological features identified in tiles to entire whole slide images, we estimated the presence of two significant and easily recognisable features (spindle cells, and fibrotic tissue) using the visual-language model CONCH [65]. This demonstrated that spindle cell shape was indeed characteristic of Ca A1, and interestingly was also common in supra-carcinoid samples, and further confirmed that the absence of fibrotic tissue was associated with Ca B (Supplementary Fig. S15).

For an illustration of the overall approach, we display three tumours correctly classified by the deep learning model (probability > 0.95), highlighting the regions given most attention by the model, and their morphological features. The algorithm was highly focussed on tiles with spindle cells and solid morphology to predict the Ca A1 tumour, on regions with organoid tissue architecture to predict the Ca A2 tumour, and on regions with round cells and cartilage to predict the Ca B tumour (Fig. 6a).

Opportunities for implementing a more clinically relevant morpho-molecular classification

Several previous studies have investigated whether molecular features may better capture lung NET diversity than the current grading system, including Laddha et al. [8], whose LC1, LC2, and LC3 groups were found previously to correspond to Ca A1, Ca B, and Ca A2, respectively [7]. We therefore sought to reconcile these proposals with the molecular groups characterised in the current study. Recently, Werr et al. showed that high expression of *TERT* was predictive of prognosis independently of tumour grade [66]. Here we found both tumour grade and molecular group to be associated with *TERT* expression whereby grade-2 tumours were significantly more frequently *TERT* high than grade-1 (61% versus 29%), and Ca A2 tumours were significantly more often *TERT* low than Ca A1, Ca B, or sc-enriched tumours (83% versus 52%, 50% and 31%, respectively, Fig. 6b, Supplementary Fig. S16a-b, Supplementary Table S41). Analysis of cis-regulatory elements led Davis et al. to propose three regulatory subtypes of lung NETs: Proneural, HNF + , and Luminal [67]. We found that almost all Ca A1 tumours were of the Proneural subtype ($n = 97/109$), characterised by high expression of *ASCL1*. Ca A2 corresponded to the HNF + subtype ($n = 87/89$), characterised by high expression of HNF genes, including *HNF1A* and *HNF4A*, and the neuronal TF *OTP*. The Luminal subtype, typified by high HNF gene expression but low levels of *OTP*, corresponded to Ca B ($n = 55/62$). Whilst two sc-enriched were Proneural and one Luminal, most did not correspond to any subtype, however almost all were *OTP*-low ($n = 11/13$, Fig. 6b, Supplementary Table S42). Given the similarity between supra-carcinoid and lung NEC molecular profiles [6, 7], we also examined the alignment between lung NETs and proposed markers for TF-driven subtypes of SCLC.

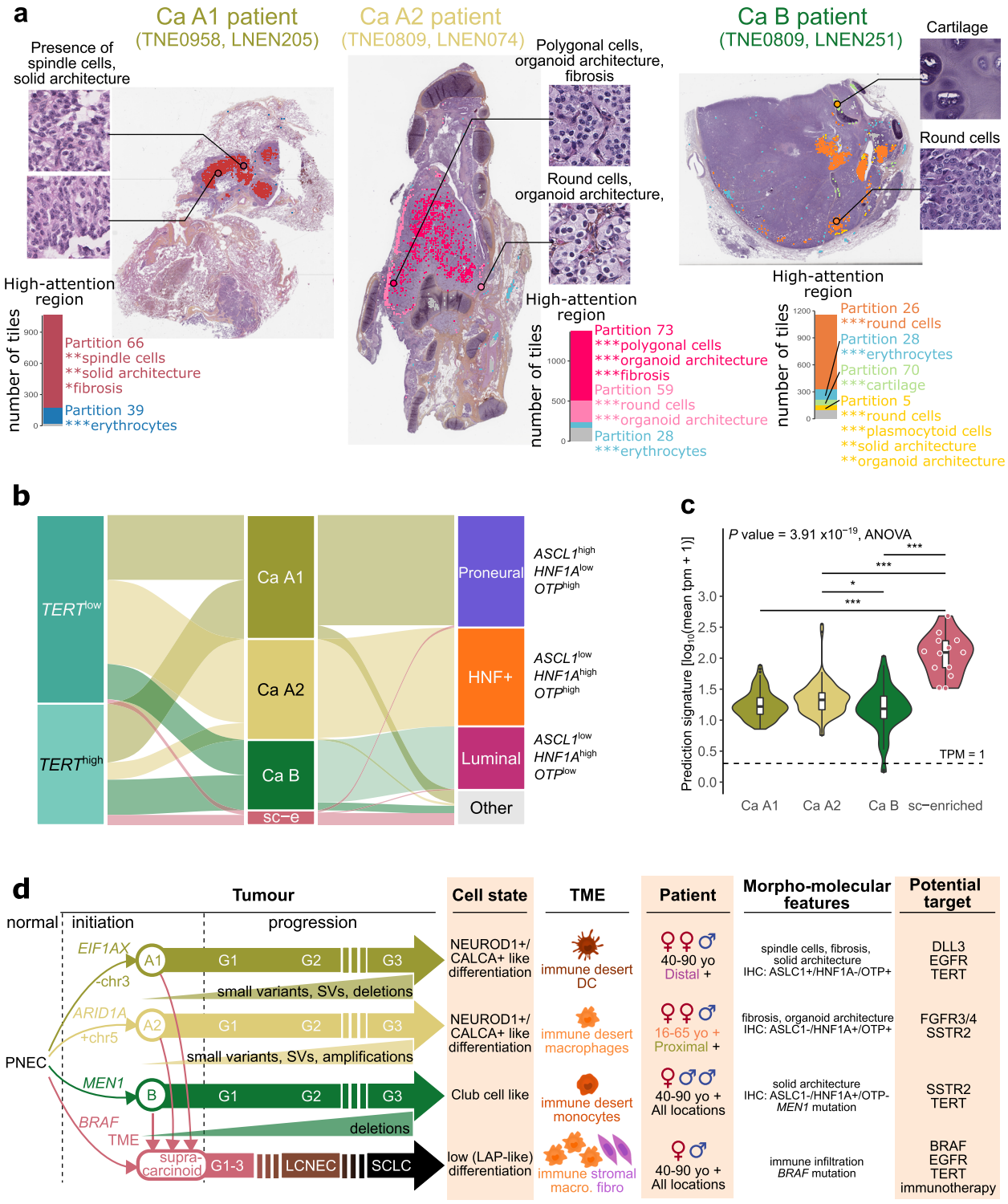

Fig. 6 (See legend on next page.)

(See figure on previous page.)

Fig. 6 Presentation of a biologically grounded and clinically relevant morpho-molecular classification. **a** Example of how the morphological criteria identified by deep learning could help diagnose patient molecular group. Coloured squares correspond to high-attention tiles identified by RoFormer-MIL to predict molecular groups. Colours represent different partitions, and barplots display the number of tiles from the different partitions in these high-attention regions. Example tiles from partitions along with their consensus pathological annotations from two independent pathologists are also represented, where stars correspond to the significance of the association between partitions and annotations. * $0.01 < q$ value < 0.05; ** $0.001 < q$ value ≤ 0.01; *** q value ≤ 0.001. **b** Alluvial plots comparing the proposed four-group molecular classification with other published classifications, determined by marker gene expression; box sizes correspond to sample sizes in the study cohort, $n = 273$. **c** Distribution of mean expression (in log10(TPM + 1) of a panel of 18 genes that capture a T-cell inflamed phenotype and is associated with response to PD-1 inhibitor pembrolizumab by molecular group. $n = 273$, TPM, transcripts per kilobase million. Pair-wise comparisons performed with t-tests. * $0.01 < P$ value < 0.05; ** $0.001 < P$ value ≤ 0.01; *** P value ≤ 0.001. **d** Schematic depicting the molecular, clinical, and morphological characteristics of the proposed morpho-molecular classification for lung NETs. PNEC, pulmonary neuroendocrine cell (putative cell of origin); TME, tumour microenvironment; G1, grade-1; G2, grade-2; G3, grade-3; SVs, structural variants; LCNEC, large cell neuroendocrine carcinoma; SCLC, small cell lung cancer; LAP, lower airway progenitor; DC, dendritic cell; macro, macrophage; fibro, fibroblast; yo, years old

SCLC-A, SCLC-N, SCLC-P, and SCLC-I are characterised by elevated *ASCL1*, *NEUROD1*, or *POU2F3* expression, or low expression of all three alongside an inflamed gene signature and *YAP1* expression, respectively [68]. Our analysis revealed that Ca A1, Ca A2, and Ca B lung NETs either fell into the SCLC-A subtype (mainly Ca A1, aligning with the proneural lung NET subtype), or were negative for all three markers (*ASCL1*, *NEUROD1*, *POU2F3*), however, approximately half of Ca A1 and Ca A2 tumours also expressed low levels of *YAP1*. In the case of sc-enriched, they displayed the highest *YAP1* expression and inflamed score (SCLC-I), but interestingly approximately half were also *ASCL1*-high (Supplementary Fig. S16c, Supplementary Table S43). Also, as previously reported [6, 48], bona fide SCLC *TP53* and *RB1* alterations were rare or non-existent in lung NETs (Supplementary Fig. S16c, Supplementary Tables S25 & S28).

It has been suggested that the current histological grading system for lung NETs does not adequately capture the variability present within lung NETs, and is lacking in terms of clinical utility, both for prognostication and identification of targetable molecular features for treatment [4, 5, 8, 9, 13]. Importantly, clinically relevant features were also identified in the molecular groups including differences in survival and potential therapeutic vulnerabilities. Ten-year overall survival rates were 86% for Ca A1, 83% for Ca A2, 70% for Ca B, and 60% for sc-enriched, and paired analysis indicated poorer overall survival for Ca B and sc-enriched compared with Ca A2 (Supplementary Table S6). Sc-enriched also had poorer overall survival compared with Ca A2 after adjusting for sex and stage, but not tumour grade (features that were additionally associated with survival). In contrast, grade-2 had poorer overall survival than grade-1 when adjusting for sex, stage, or molecular group (Supplementary Table S6). A number of approved and emerging targeted therapies have recently been reported on for neuroendocrine neoplasms including DLL3 [69], FGFR3/4 [67], and EGFR [11] inhibitors, somatostatin analogues (*SSTR2*) [70, 71], and alkylating agents (*MGMT*) [72, 73]. Such therapies are associated with expression-based predictive markers [13], and given the described biological variation between molecular groups we therefore assessed whether treatment response marker expression profiles also differed across the cohort. While no markers were significantly differentially expressed between grade-1 and grade-2 tumours, they did differ by molecular group. Delta-like protein 3 (*DLL3*), a direct downstream target of the Ca A1 core upregulated gene *ASCL1*, was expressed at a higher level in Ca A1 than in all other groups. Ca A1 also had the highest expression of *EGFR*, along with sc-enriched tumours. *FGFR4* was most highly expressed in Ca A2, whilst *FGFR3* was highest in Ca A2 and sc-enriched. Ca A2 and Ca B shared high expression of *SSTR2*, and finally *MGMT* was slightly elevated in sc-enriched tumours compared with Ca A1 and Ca A2 (Supplementary Fig. S17, Supplementary Table S43). We additionally examined the expression a panel of 18 genes that capture a T-cell inflamed phenotype and is associated with response to PD-1 inhibitor pembrolizumab in nine different cancer types [74]. Mean expression was significantly higher in sc-enriched than other molecular groups, a promising finding given the higher expression observed in pembrolizumab responders [74] (Fig. 6c, Supplementary Table S44). Grade-2 tumours also showed a modest increase in the PD-1 inhibitor response signature compared to grade-1 (1.7-fold higher), but this difference was smaller than that observed between sc-enriched and other molecular groups (5 to sevenfold higher, Supplementary Figure S16d, Supplementary Table S44).

Despite its potential, a key challenge to any molecular classification lies in its implementation in clinical practice. To address this, we assessed two methods suitable for different resource settings. Firstly, Leunissen et al. [9] demonstrated that a combination of ASCL1, HNF1A, and OTP protein expression could accurately classify a small cohort of lung NETs into their known molecular group (Ca A1, Ca A2, and Ca B) based on a subset of our series ($n = 15$). Applying the immunohistochemistry (IHC) panel to 90 additional samples in our series ($n = 30$ each of Ca A1, Ca A2, and Ca B) resulted in a predicted molecular group for 77% of samples. Of the classified samples, 99% were correctly predicted, and only one was

misclassified (Supplementary Fig. S18a-b, Supplementary Table S45). Although not included in the IHC experiment, gene expression analysis of *ASCL1*, *HNF1A*, and *OTP* in supra-carcinoids demonstrated unique profiles such that ten out of 13 tumours did not match any of the Ca A1, Ca A2, or Ca B patterns (Supplementary Table S42). Subsequently, using a selection of the deep learning-identified morphological features: spindle cells, organoid and solid architecture, and fibrosis, the unclassified/misclassified cases from the IHC experiment ($n = 22$) were reassessed, and nine were able to be correctly grouped, despite being more complex cases (Supplementary Fig. S18c, Supplementary Table S45). In total, using the three-protein IHC panel and the morphological signature of the molecular groups we managed to correctly assign to their molecular groups 77 out of 90 samples assessed.

Secondly, we evaluated PACMOS, our publicly available R package designed to classify new samples with single or multi-omic data into the four molecular groups (defined in this study). Cross validation within our cohort demonstrated an accuracy of 100% in assigning study samples to one of the four molecular groups when using both RNA sequencing and DNA methylation array data, 98.9% using RNA sequencing data alone, and 98.8% using DNA methylation data alone (Supplementary Table S46). To assess its applicability to external datasets, we applied PACMOS to publicly available lung NET RNA sequencing data from Laddha et al. [8]. Among 29 patient samples, PACMOS assignments were concordant with expression-based subtypes previously reported by Laddha et al., all LC1 samples were assigned to Ca A1, all LC2 to Ca B, and all LC3 to Ca A2 (Supplementary Fig. S19a, Supplementary Table S46). Finally, we projected an additional longitudinal sample from a supra-carcinoid patient included in the study cohort, obtained two years after initial diagnosis, this sample was also classified as sc-enriched (Supplementary Fig. S19b, Supplementary Table S46). Together, these results indicate that PACMOS can classify new lung NET samples with available transcriptomic and/or methylation data, providing a practical tool for translational research studies.

Discussion

Prior to this study, we and others had introduced the concept of molecular groups of lung NETs (Ca A1, Ca A2, and Ca B) that were in opposition to the current WHO classification of grade-1 (typical) and grade-2 (atypical) tumour types [6, 8, 67]. In this study we applied archetype analysis to latent factors representing multi-omic variation within a large cohort of lung NETs, identifying a fourth group encompassing almost all instances of supra-carcinoids. This supra-carcinoid enriched group displayed a more disrupted genomic profile, an immune rich microenvironment, more frequent pleural invasion, and may be more clinically aggressive. The molecular groups Ca A1, Ca A2, and Ca B are likely determined early in tumorigenesis by genomic events, and were highly spatially stable, however the evidence for early determination of supra-carcinoids was more mixed. Whilst we identified a supra-carcinoid specific driver alteration, *BRAF* V600E, though present in only two samples, many tumours also harboured driver alterations characteristic of other molecular groups, and also contained regions with profiles matching these other groups, suggesting that supra-carcinoids may evolve from Ca A1, Ca A2, or Ca B.

Cell of origin analyses did not indicate a unique precursor for each group but were suggestive of differences in tumour development. The high proportion of differentiated pulmonary NE cells present in Ca A1, in combination with the proneural nature of its putative master transcription factors *ASCL1* and *MYLT1* [59, 61, 62], is suggestive of a group of tumours arising from a pulmonary NE cell of origin that has undergone limited dedifferentiation during tumourigenesis. In parallel, recent studies have reported specific enrichment within a Ca A1-like patient group (older women with peripheral lung NETs with high *ASCL1* expression) for the preinvasive condition diffuse idiopathic pulmonary neuroendocrine cell hyperplasia (DIPNECH) [9, 75, 76]. It is plausible that DIPNECH predisposes patients to the development of Ca A1 lung NETs specifically, and the Ca A1 NE-like phenotype is reflective of a possible relationship with hyperplastic NE precursor lesions. In contrast, Ca B had a high proportion of club cells, shown in animal models to play an important role in repair of airway epithelial cells following injury, and to contribute to the removal of xenobiotic compounds within the lung [77]. This was in line with the upregulation of several *UGT* genes within Ca B, that are also crucial for the elimination of xenobiotic compounds [78], and suggests that environmental exposures, such as smoking, may be specifically involved in the development of Ca B tumours. The finding that the pulmonary NE precursor, LAP cells [38], were most abundant in sc-enriched tumours, and were very rarely present in the other molecular groups, suggests that at least a subset of supra-carcinoids are in an undifferentiated, stem-like cellular state with loss of neuroendocrine phenotype. Finally, the co-localisation of LAP and sc-enriched regions with macrophages and fibroblasts, and the significant interaction between markers of macrophages and LAP cells, suggests that the tumour microenvironment may be key to supra-carcinoid development, although it may not be essential for maintaining their phenotype and growth [46].

Lung NENs are currently divided into low-grade NETs and high-grade NECs, however the molecular similarity between supra-carcinoids and lung NECs does lend weight to the idea that NETs and NECs represent two

ends of a spectrum of highly stable tumour groups rather than two completely unrelated diseases [44, 45]. Supporting this hypothesis is the recent publication of so-called atypical SCLC tumours which demonstrated the possibility of NEC development through transformation of a lung NET via chromothripsis [49]. Our case report on LNET10 provides additional evidence that a low-grade NET may progress to a high-grade NEC in the context of chromothripsis, and our reanalysis of the atypical SCLC [49] data suggests that such tumours may in fact be fully transformed supra-carcinoids. Our observations on the development of supra-carcinoids, whether that be through evolution of other molecular groups or de novo appearance, their stability over time or capacity for high-grade transformation and the potential mechanisms involved, be that chromothripsis and/or changes in tumour microenvironment and neuroendocrine cell state, have generated hypotheses that will need to be tested in future mechanistic and longitudinal studies. Furthermore, whether supra-carcinoids represent a transitional entity, or a distinct morphological subtype of lung NETs, remains to be evaluated, including by expert pathologists in purposely designed studies.

Finally, the four molecular groups capture differences in epidemiological and biological features that are not represented by the current histological system, which is more a measure of tumour progression. Whilst our findings do not provide direct evidence of the therapeutic value of the molecular groups, they highlight the limitations of relying solely on histological subtypes which may obscure biologically relevant differences. Thus, as supported by the differences in protein expression identified by Leunissen et al. [9], consistent with our gene expression findings, the molecular groups provide a plausible patient stratification framework for future clinical trials. Importantly, this molecular classification has the potential to be implemented in both the research and clinical settings, either through the use of software (PACMOS) or classical cancer diagnostic methods (IHC panel combined with morphology). However further refinement is certainly needed, specifically to ensure reproducibility in assays between settings, and to more concretely determine diagnostic morphological features, particularly for supra-carcinoid tumours.

Conclusions

We identify the fourth distinct molecular group of lung NETs as being supra-carcinoid enriched (sc-enriched), and prove that each of the molecular groups (Ca A1, Ca A2, Ca B, and sc-enriched) has unique aetiology, clinical and epidemiological features, molecular profiles, microenvironmental niches, and evolutionary histories, suggestive of different diseases that should be tackled with different clinical approaches (Fig. 6d). These molecular groups are independent of but complementary to the current WHO classification, with the former more accurately reflecting tumour biology to guide future clinical trial design, and the latter capturing tumour progression and remaining key for prognostication. These data raise awareness about the existence of the supra-carcinoid phenotype and provide a window into the so far unrecognised lung NEN plasticity.

Abbreviations

CAF	Cancer associated fibroblast
chr	Chromosome
CNV	Copy number variation
DNA	Deoxyribonucleic acid
HE/HES	Haematoxylin eosin/haematoxylin eosin saffron
IHC	Immunohistochemistry
LAP	Lower airway progenitor
LCNEC	Large cell neuroendocrine carcinoma
MIF	Macrophage migration inhibitory factor
NEC	Neuroendocrine carcinoma
NEN	Neuroendocrine neoplasm
NET	Neuroendocrine tumour
PDTO	Patient-derived tumour organoid
sc-enriched	Supra-carcinoid enriched
TF	Transcription factor
TPM	Transcripts per kilobase million
SCLC	Small cell lung cancer
WHO	World Health Organisation

Supplementary Information

The online version contains supplementary material available at https://doi.org/10.1186/s12943-026-02721-7.

Supplementary Material 1: Supplementary Methods.

Supplementary Material 2: Supplementary Figures.

Supplementary Material 3: Supplementary Tables.

Acknowledgements

The lungNENomics project is part of the Rare Cancers Genomics initiative (www.rarecancersgenomics.com/) led by the Computational Cancer Genomics team at the IARC (https://www.iarc.who.int/teams-ccg/). This work is also part of the European Neuroendocrine Tumor Society (ENETs) lung task force. We thank the Hospices Civils de Lyon (CRB-HCL BB-0033-00046) and Centre Léon Bérard (CRB-CLB BB-0033- 00050) biobanks in Lyon, as well as Côte d'Azur University's biobank (BB-0033-00025) in Nice, France, all authorised by the French Ministry of Research, for sharing human biological samples and associated data. We thank the 12 centres that voluntarily participated in the lungNENomics project by providing one FFPE block per patient: The Tumour Bank of the François Baclesse Centre in Caen (France), the Institut für Diagnostik und Forschung in Pathologie of the Medical University of Graz (Austria), the Department of Biopathology of the Léon Bérard Centre in Lyon (France), the Institute of Pathology of the Hospices civils de Lyon (France), the Department of Surgical Oncology of St Vincent's Hospital in Melbourne (Australia), the Department of Oncology and Haemato-Oncology of the University of Milan (Italy), the Department of Biopathology at the Nancy Regional Hospital (France), the Laboratory of Clinical and Experimental Pathology at the Pasteur Hospital in Nice (France), the Departments of Pathology and Oncology at Oslo University Hospital (Norway), the Pathology Department at the Cochin Hospital in Paris (France), the Oncology Unit at the IRCCS Cas Sollievo della Sofferenza Foundation in Rotondo (Italy), and the Oncology Department at the University of Turin (Italy). The results published here are in part based upon data generated by the TCGA Research Network: https://www.cancer.gov/tcga. We also would like to acknowledge the contribution of Jean-Philippe Berthet, Frederic Bibeau, Cécile Blanc Fournier, Anne Boland, Christelle Bonnetaud, Charlotte Cohen, Concetta Martina Di Micco, Jean Philippe Lerochais, Nathalie Rousseau, and Giovanna Sabella.

Authors' contributions
Conceptualization: N.A., M.F., L.F–C. Data curation: A.S–O., E.M., N.C., C.V., A.DG., N.A. Formal analyses: A.S–O., E.M., N.C., Y.L., C.V., A.DG., La.Ma., Z.L., L.K., T.M.D., R.B-E., A.G-P., M.L.M., E.L., Li.M., Li.B.,V.C., N.A. Funding acquisition: N.A., M.F., L.F–C. Investigation: T.vW., L.M.H., La.Mo., J.A., C.D., A.C., Cy.C., F.D., N.G., A.G., C.P., S.T-E., La.C., M.V., J-M.V.,E.C., A.M-L., Lu.B., G.P., M.G.P., S.L. Methodology: E.M., N.A. Project administration: A.S–O., M.F., L.F–C. Software: A.S–O., E.M., N.C., Y.L., A.DG., La.Ma., Z.L., L.K., N.A. Resources: G.A., O.T.B., G.C., V.T.dM., J-F.D., A-M.C.D., E.F., P.G., P.H., V.H., S.L., M.L-I., M.M., L.A.M., C.P., G.P., H.P., L.R., A.S., W.B., J.vdB., M.T., E.J.M.S., S.T-E., T.W., G.M.W., La.C., C.C., M.V., J-M.V., Lu.B., M.G.P., S.L. Supervision: A.I-C., N.L-B., S.P-A., J.K., E.J.M.S., S.T-E., J.P.C., Li.C., N.G., S.L., J.D., T.D., N.A., M.F., L.F–C. Validation: A.S–O., E.M., N.C., N.A. Visualization: A.S–O., E.M., Y.L., La.Ma., T.M.D., N.A. Writing – original draft: A.S–O., E.M., N.C., Y.L., La.Ma., N.A., M.F., L.F–C. Writing – review & editing: all authors.

Funding
This work was supported by HPC resources from GENCI- IDRIS (grant numbers 2022-AD011012172R1 and 2024- AD010315173). This work was also supported by the Neuroendocrine Tumor Research Foundation (NETRF) (Investigator Award 2019 to L.F–C., Accelerator Award 2025 to L.F–C., Investigator Award 2022 to M.F., Investigator Award 2023 to T.D., Mentored Award 2022 to J.D., Mentored Award 2023 to N.A.), Worldwide Cancer Research (WCR) (grant numbers 21–0005 and 26–0008 to L.F–C.), the French National Cancer Institute (INCa-PRT-K-17–047 to L.F–C., INCa-DGOS-INSERM-ITMO cancer_18003 LYRICAN +, and LABREXCMP24-001 – Inca_18791), PhD fellowships from the French League Against Cancer (to Y.L. and La.Ma.), a collaborative research grant from the France-Stanford center for interdisciplinary studies (to N.A.), European Neuroendocrine Tumor Society (Translational Medicine Fellowship 2021 to J.D), Dutch Cancer Society (10956, 2017 to J.D., and to E.J.M.S), Ricerca Corrente Program, Italian Ministry of Health (to L.A.M), "5 × 1000" voluntary contributions to Fondazione IRCCS Casa Sollievo della Sofferenza (to L.A.M.), Spanish Ministry of Science and Innovation [MICIU PID2022-136227OB-I00 (to J.P.C.), Agence Nationale de la Recherche under the France 2030 programme (ANR-23-IAHU-0007, to P.H), l'Agence Nationale de Recherche (ANR-18-CHR3-0002–01, ANR-20-IADJ-0001–01, ANR-21-FAI1-0009–01, to Li.C), Axelera (Project Structurant pour la Compétitivité FAIR WASTE, to Li.C), the Italian Association for Cancer Research (AIRC; IG21431 to L. R.)

Data availability
Sequencing data are available on the European Genome-Phenome archive (study EGAS00001005979). Previously published data from Alcala et al. 2019 [6] and Dayton et al. 2023 [46] are also available on EGA (studies EGAS00001003699 and EGAS00001005752, respectively). The code used are available on IARC's github repository https://github.com/IARCbioinfo/ under open-source licenses. In particular, the code to process the sequencing data (QC, alignment, variant calling) are listed at https://github.com/IARCbioinfo/IARC-nf, the code to process the whole-slide images are available at https://github.com/IARCbioinfo/WSIPreprocessing and https://github.com/IARCbioinfo/LNENBarlowTwins, and the code to analyse the data and reproduce the main results (Figures) is available on the github repository https://github.com/IARCbioinfo/MS_lungNENomics. Additionally, an accompanying data note describes in further detail data processing and quality control.

Declarations

Ethics approval and consent to participate
This study was approved by the International Agency for Research on Cancer Ethics Committee (project number 19–07).

Consent for publication
Not applicable.

Competing interests
Where authors are identified as personnel of the International Agency for Research on Cancer/World Health Organization, the authors alone are responsible for the views expressed in this article and they do not necessarily represent the decisions, policy or views of the International Agency for Research on Cancer/World Health Organization. Nicolas Girard has research support from Abbvie, Amgen, AstraZeneca, Beigene, Boehringer Ingelheim, Bristol Myers Squibb, Daiichi-Sankyo, Gilead, Hoffmann-La Roche, Janssen, LeoPharma, Lilly, Merk Serono, Merck Sharp & Dohme, Novartis, Sanofi, Sivan; he also has consultative services for Abbvie, Amgen, AstraZeneca, Beigene, Bristol Myers Squibb, Daiichi-Sankyo, Gilead, Ipsen Hoffmann-La Roche, Janssen, LeoPharma, Lilly, Merck Sharp & Dohme, Mirati, Novartis, Pfizer, Pierre Fabre, Sanofi, Sivan Takeda; and he participates on a data safety monitoring board for Hoffmann-La Roche. Ernst-Jan M Speel has grant support from Pfizer, and participates on advisory boards for AstraZeneca, GSK, Johnson & Johnson, and Illumina.

Author details
[1]Computational Cancer Genomics Team, Genomic Epidemiology Branch, International Agency for Research On Cancer (IARC-WHO), 25 Avenue Tony Garnier, Lyon CEDEX 07 69372, France
[2]European Molecular Biology Laboratory, Barcelona, Spain
[3]Instituto de Ciencias de La Ingeniería, Universidad de O'Higgins, Rancagua, Chile
[4]Centro UOH de Bioingenieria (CUBI), Universidad de O'Higgins, Rancagua, Chile
[5]Centro de Modelamiento Matemático UMI-CNRS 2807, Santiago, Chile
[6]Department of Computational Biology, Cornell University, New York, USA
[7]Department of Pathology, GROW Research Institute for Oncology and Reproduction, Maastricht University Medical Centre, Maastricht, The Netherlands
[8]Otto Loewi Research Centre, Lung Research Cluster, Medical University of Graz, Graz, Austria
[9]Maimonides Biomedical Research Institute of Cordoba (IMIBIC), Cordoba, Spain
[10]Department of Cell Biology, Physiology and Immunology, University of Cordoba, Cordoba, Spain
[11]Reina Sofia University Hospital, Cordoba, Spain
[12]Institute for Research in Biomedicine (IRB Barcelona), The Barcelona Institute of Science and Technology, Barcelona, Spain
[13]Centro de Investigación Biomédica en Red en Cáncer (CIBERONC), Instituto de Salud Carlos III, Madrid, Spain
[14]Department of Medicine and Life Sciences, Universitat Pompeu Fabra, Barcelona, Spain
[15]Department of Biology, Stanford University, Stanford, CA, USA
[16]Sante Fe Institute, Sante Fe, USA
[17]Interdisciplinary Department of Medicine, University of Bari "Aldo Moro", Bari, Italy
[18]Stanford Cancer Institute, School of Medicine, Stanford University, Stanford, CA, USA
[19]Department of Internal Medicine, Division of Oncology, Medical University of Graz, Graz, Austria
[20]Max Delbrück Center for Molecular Medicine in the Helmholtz Association, Berlin, Germany
[21]Berlin Institute of Health, Charité-Universitätsmedizin Berlin, Berlin, Germany
[22]Cancer Genomic Platform, Centre de Recherche en Cancérologie de Lyon (CRCL) INSERM U1052-CNRS UMR5286, Université de Lyon, Université Claude Bernard Lyon1, Centre Léon Bérard, Lyon, France
[23]Institute of Clinical Medicine, University of Oslo, Oslo, Norway
[24]Section of Oncology, Drammen Hospital, Vestre Viken Hospital Trust, Drammen, Norway
[25]Institute for Cancer Research, Oslo University Hospital, Oslo, Norway
[26]Epigenomics and Mechanisms Branch, International Agency for Research On Cancer (IARC-WHO), Lyon, France
[27]Department of Pathology and Laboratory Medicine, First Pathology Division, Fondazione IRCCS Istituto Nazionale Dei Tumori, Milan, Italy
[28]CNRS 5286, Lyon 1 University & Department of Biopathology, Pathology Research Platform, Cancer Research Center of Lyon, INSERM 1052, CNR MESOPATH NETMESO, Centre Léon Bérard, Lyon, France
[29]Department of Pathology, Hôpital Marie-Lannelongue, Groupe Hospitalier Paris Saint Joseph, Le Plessis Robinson, France
[30]Centre National de Recherche en Génomique Humaine (CNRGH), CEA-Institut de Biologie François Jacob, Université Paris-Saclay, Evry, France
[31]Department of Pulmonary Medicine, Erasmus MC Cancer Institute, University Medical Center, Rotterdam, The Netherlands
[32]Paris Saclay University, Gif-Sur-Yvette, France
[33]Department of Radiological, Oncological and Pathological Sciences, Sapienza University of Rome, Rome, Italy

[34]Unit of Pathology, Fondazione IRCCS Casa Sollievo Della Sofferenza, San Giovanni Rotondo, Italy
[35]IHU RespirERA, Laboratory of Clinical and Experimental Pathology, FHU OncoAge, Côte d'Azur University, Nice, France
[36]Center of Biological Resources BB-0033-00035, University Hospital of Nancy, Vandœuvre-lès-Nancy, France
[37]Institució Catalana de Recerca I Estudis Avançats (ICREA), Barcelona, Spain
[38]Department of Pathology, Oslo University Hospital, Oslo, Norway
[39]Laboratory of Oncology, Fondazione IRCCS Casa Sollievo Della Sofferenza, San Giovanni Rotondo, Italy
[40]Hospices Civils de Lyon Biobank (CRB HCL), Tissu-Tumorothèque Est, Lyon, France
[41]Pathology Department, Caen University Hospital, Normandy University, Caen, France
[42]Pathology Institute for Diagnostics and Research, Medical University Graz, Graz, Austria
[43]Department of Experimental Oncology, Fondazione IRCCS - Istituto Nazionale Dei Tumori, Milan, Italy
[44]Department of Thoracic Oncology, Netherlands Cancer Institute, Amsterdam, The Netherlands
[45]Department of Pathology, Netherlands Cancer Institute, Amsterdam, The Netherlands
[46]Department of Medical Oncology, Netherlands Cancer Institute, Amsterdam, The Netherlands
[47]Department of Pathology and Clinical Bioinformatics, Erasmus Medical Center, Rotterdam, The Netherlands
[48]Plateforme de Gestion Des Echantillons Biologique, Centre Léon Bérard, Cancer Research Center of Lyon, Université de Lyon, Université Claude Bernard Lyon 1, INSERM 1052, CNRS 5286, Lyon, France
[49]Gastroenterology and Technologies for Health, INSERM UMR 1052 CNRS UMR 5286, Cancer Research Center of Lyon, University of Lyon, Lyon, France
[50]Department of Medical Oncology, Edouard Herriot Hospital, Hospices Civils de Lyon, Lyon, France
[51]University of Melbourne, Melbourne, Australia
[52]Department of Surgery, St Vincent's Hospital, Melbourne, Australia
[53]CIBER Physiopathology of Obesity and Nutrition (CIBERobn), Cordoba, Spain
[54]Department of Pathology, Groupe Hospitalier Est, Hospices Civils de Lyon, Bron, France
[55]Department of Mathematics and Informatics, Ecole Centrale de Lyon, Lyon, France
[56]Institut Universitaire de France (IUF), Paris, France
[57]CISTAR Team, Cancer Research Center of Lyon, INSERM U1052, CNRS UMR5286, Université de Lyon, 8 Université Lyon 1, Centre Léon Bérard, Lyon, France
[58]Department of Oncology, University of Turin at San Luigi Hospital, Orbassano, Turin, Italy
[59]Institut Curie, Paris, France
[60]Université de Versailles Saint-Quentin-en-Yvelines, Paris Saclay, Versailles, France
[61]EURACAN, Lyon, France
[62]Department of Biopathologie, Nancy University Hospital, Nancy, France
[63]Department of Pathology, Hospital Universitario 12 de Octubre, Universidad Complutense de Madrid, Madrid, Spain
[64]Instituto de Investigación Sanitaria Hospital 12 de Octubre (imas12), CIBERONC, Madrid, Spain
[65]Department of Pathology, Cochin Hospital, APHP Paris Centre, Paris City University, Paris, France
[66]Department of Pathology, Hospital Graz II, Graz, Austria
[67]Department of Pathology, Medical University of Vienna, Vienna, Austria
[68]Department of Oncology and Hemato-Oncology, University of Milan, Milan, Italy
[69]Department of Oncology, University of Turin, Turin, Italy
[70]Grenoble Alpes University, Grenoble, France
[71]Department of Biopathology, Léon Bérard Cancer Center, Lyon, France

Received: 27 February 2026 / Accepted: 11 June 2026
Published online: 27 August 2026

References

1. WHO Classification of Tumours Editorial Board. Thoracic tumours 5th edn, vol. vol. 5. Lyon: International Agency for Research on Cancer; 2021.
2. Nicholson AG, et al. The 2021 WHO Classification of Lung Tumors: Impact of Advances Since 2015. J Thorac Oncol. 2022;17:362–87.
3. Tsao MS, Nicholson AG, Maleszewski JJ, Marx A, Travis WD. Introduction to 2021 WHO Classification of Thoracic Tumors. J Thorac Oncol. 2022;17:e1–4.
4. Swarts DRA, et al. Interobserver variability for the WHO classification of pulmonary carcinoids. Am J Surg Pathol. 2014;38:1429–36.
5. Mathian É, et al. Assessment of the current and emerging criteria for the histopathological classification of lung neuroendocrine tumours in the lungNENomics project. ESMO Open. 2024;9:103591.
6. Alcala N, et al. Integrative and comparative genomic analyses identify clinically relevant pulmonary carcinoid groups and unveil the supra-carcinoids. Nat Commun. 2019;10:3407.
7. Gabriel AAG, et al. A molecular map of lung neuroendocrine neoplasms. Gigascience. 2020;9:giaa112.
8. Laddha SV, et al. Integrative genomic characterization identifies molecular subtypes of lung carcinoids. Cancer Res. 2019;79:4339–47.
9. Leunissen DJG, et al. Identification of defined molecular subgroups on the basis of immunohistochemical analyses and potential therapeutic vulnerabilities of pulmonary carcinoids. J Thorac Oncol. 2025;20:451–64.
10. Sun TY, Hendifar A, Padda SK. Lung Neuroendocrine Tumors: How Does Molecular Profiling Help? Curr Oncol Rep. 2022;24:819–24.
11. Boilève A, et al. Molecular profiling and target actionability for precision medicine in neuroendocrine neoplasms: real-world data. Eur J Cancer. 2023;186:122–32.
12. Miyanaga A, et al. Whole-exome and RNA sequencing of pulmonary carcinoid reveals chromosomal rearrangements associated with recurrence. Lung Cancer. 2020;145:85–94.
13. Fernandez-Cuesta L, et al. Basic science and translational implications of current knowledge on neuroendocrine tumors. J Clin Invest. 2025;135:e186702.
14. Fernandez-Cuesta L, et al. Spotlight on Small-Cell Lung Cancer and Other Lung Neuroendocrine Neoplasms. Am Soc Clin Oncol Educ Book. 2023;43:e390794.
15. Hermans BCM, et al. Unique Metastatic Patterns in Neuroendocrine Neoplasms of Different Primary Origin. Neuroendocrinology. 2021;111:1111–20.
16. Rekhtman N, et al. Stage IV lung carcinoids: spectrum and evolution of proliferation rate, focusing on variants with elevated proliferation indices. Mod Pathol. 2019;32:1106–22.
17. Argelaguet R, et al. MOFA+: A statistical framework for comprehensive integration of multi-modal single-cell data. Genome Biol. 2020;21:111.
18. Kalson L, et al. A multi-omic, spatial, and whole-slide image dataset of lung neuroendocrine tumours from the lungNENomics cohort. bioRxiv 2026.05.12.724489. 2026. https://doi.org/10.64898/2026.05.12.724489.
19. Hausser J, Alon U. Tumour heterogeneity and the evolutionary trade-offs of cancer. Nat Rev Cancer. 2020;20:247–57.
20. Hausser J, et al. Tumor diversity and the trade-off between universal cancer tasks. Nat Commun. 2019;10:5423.
21. Morrison ML, et al. Variability of mutational signatures is a footprint of carcinogens. medRxiv 2023.11.23.23298821. 2023. https://doi.org/10.1101/2023.11.23.23298821.
22. Hanahan D, Weinberg RA. Hallmarks of cancer: the next generation. Cell. 2011;144:646–74.
23. Hanahan D. Hallmarks of Cancer: New Dimensions. Cancer Discov. 2022;12:31–46.
24. Bielski CM, et al. Genome doubling shapes the evolution and prognosis of advanced cancers. Nat Genet. 2018;50:1189–95.
25. Venet D, Dumont JE, Detours V. Most random gene expression signatures are significantly associated with breast cancer outcome. PLoS Comput Biol. 2011;7:e10002240 .
26. Finotello F, et al. Molecular and pharmacological modulators of the tumor immune contexture revealed by deconvolution of RNA-seq data. Genome Med. 2019;11:34.
27. Sturm G, et al. Comprehensive evaluation of transcriptome-based cell-type quantification methods for immuno-oncology. Bioinformatics. 2019;35:i436–45.
28. Cassetta L, Pollard JW. A timeline of tumour-associated macrophage biology. Nat Rev Cancer. 2023;23:238–57.
29. Combes AJ, et al. Discovering dominant tumor immune archetypes in a pan-cancer census. Cell. 2022;185:184-203.e19.

30. Combes AJ, Samad B, Krummel MF. Defining and using immune archetypes to classify and treat cancer. Nat Rev Cancer. 2023;23:491–505.
31. Alvarez MJ, et al. A precision oncology approach to the pharmacological targeting of mechanistic dependencies in neuroendocrine tumors. Nat Genet. 2018;50:979–89.
32. Hofving T, et al. The Microenvironment of Small Intestinal Neuroendocrine Tumours Contains Lymphocytes Capable of Recognition and Activation after Expansion. Cancers (Basel). 2021;13:4305.
33. Greenberg J, et al. Metastatic pancreatic neuroendocrine tumors feature elevated T cell infiltration. JCI Insight. 2022;7:e160130.
34. Uccella S. Molecular Classification of Gastrointestinal and Pancreatic Neuroendocrine Neoplasms: Are We Ready for That? Endocr Pathol. 2024;35:91–106.
35. Barkley D, et al. Cancer cell states recur across tumor types and form specific interactions with the tumor microenvironment. Nat Genet. 2022;54:1192–201.
36. Bischoff P, et al. The single-cell transcriptional landscape of lung carcinoid tumors. Int J Cancer. 2022;150:2058–71.
37. Dayton T, Hartigh LD, Böttinger L, Chuva de Sousa Lopes SM, Clevers H. PO-271 Using human lung organoids to study pulmonary neuroendocrine cells. ESMO Open. 2018;3:A126.
38. Conchola AS, et al. Regionally distinct progenitor cells in the lower airway give rise to neuroendocrine and multiciliated cells in the developing human lung. Proc Natl Acad Sci U S A. 2023;120:e2210113120.
39. Jin S, et al. Inference and analysis of cell-cell communication using Cell Chat. Nat Commun. 2021;12:1088.
40. Bui TM, Wiesolek HL, Sumagin R. ICAM-1: A master regulator of cellular responses in inflammation, injury resolution, and tumorigenesis. J Leukoc Biol. 2020;108:787–99.
41. Martínez-Jiménez F, et al. A compendium of mutational cancer driver genes. Nat Rev Cancer. 2020;20:555–72.
42. Mermel CH, et al. GISTIC2.0 facilitates sensitive and confident localization of the targets of focal somatic copy-number alteration in human cancers. Genome Biol. 2011;12:R41.
43. Caravagna G, et al. Detecting repeated cancer evolution from multi-region tumor sequencing data. Nat Methods. 2018;15:707–14.
44. Pelosi G, et al. Most high-grade neuroendocrine tumours of the lung are likely to secondarily develop from pre-existing carcinoids: innovative findings skipping the current pathogenesis paradigm. Virchows Arch. 2018;472:567–77.
45. Pelosi G, et al. An in-silico analysis reveals further evidence of an aggressive subset of lung carcinoids sharing molecular features of high-grade neuroendocrine neoplasms. Exp Mol Pathol. 2024;135:104882.
46. Dayton TL, et al. Druggable growth dependencies and tumor evolution analysis in patient-derived organoids of neuroendocrine neoplasms from multiple body sites. Cancer Cell. 2023;41:2083-2099.e9.
47. Poulikakos PI, et al. RAF inhibitor resistance is mediated by dimerization of aberrantly spliced BRAF(V600E). Nature. 2011;480:387–90.
48. Fernandez-Cuesta L, et al. Frequent mutations in chromatin-remodelling genes in pulmonary carcinoids. Nat Commun. 2014;5:3518.
49. Rekhtman N, et al. Chromothripsis-Mediated Small Cell Lung Carcinoma. Cancer Discov. 2025;15:83–104.
50. George J, et al. Comprehensive genomic profiles of small cell lung cancer. Nature. 2015;524:47–53.
51. Beasley MB, et al. IASLC Update on Classification of Pulmonary Neuroendocrine Neoplasms. J Thoracic Oncol. 2026; Jun 6:103977.
52. Zhang Y, et al. Clinic and genetic similarity assessments of atypical carcinoid, neuroendocrine neoplasm with atypical carcinoid morphology and elevated mitotic count and large cell neuroendocrine carcinoma. BMC Cancer. 2022;22:321.
53. Hermans BCM, et al. Pulmonary neuroendocrine neoplasms with well differentiated morphology and high proliferative activity: illustrated by a case series and review of the literature. Lung Cancer. 2020;150:152–8.
54. Quinn AM, Chaturvedi A, Nonaka D. High-grade Neuroendocrine Carcinoma of the Lung With Carcinoid Morphology: A Study of 12 Cases. Am J Surg Pathol. 2017;41:263–70.
55. Cros J, et al. Specific Genomic Alterations in High-Grade Pulmonary Neuroendocrine Tumours with Carcinoid Morphology. Neuroendocrinology. 2021;111:158–69.
56. Kucab JE, et al. A Compendium of Mutational Signatures of Environmental Agents. Cell. 2019;177:821-836.e16.
57. Zapata L, et al. Immune selection determines tumor antigenicity and influences response to checkpoint inhibitors. Nat Genet. 2023;55:451–60.
58. Li Q, Wang K. InterVar: Clinical Interpretation of Genetic Variants by the 2015 ACMG-AMP Guidelines. Am J Hum Genet. 2017;100:267–80.
59. Travaglini KJ, et al. A molecular cell atlas of the human lung from single-cell RNA sequencing. Nature. 2020;587:619–25.
60. Reddy J, et al. Predicting master transcription factors from pan-cancer expression data. Sci Adv. 2021;7:eabf6123.
61. Kuo CS, et al. Neuroendocrinology of the lung revealed by single-cell RNA sequencing. Elife. 2022;11:e78216.
62. Mall M, et al. Myt1l safeguards neuronal identity by actively repressing many non-neuronal fates. Nature. 2017;544:245–9.
63. Zbontar J, Jing L, Misra I, LeCun Y, Deny S. Barlow Twins: Self-Supervised Learning via Redundancy Reduction. Proceedings of the 38th International Conference on Machine Learning. 2021;139:12310-12320.
64. Pochet E, Maroun R, Trullo R. RoFormer for Position Aware Multiple Instance Learning in Whole Slide Image Classification. Int Workshop Mach Learn Med Imaging. 2023:437-446.
65. Lu MY, et al. A visual-language foundation model for computational pathology. Nat Med. 2024;30:863–74.
66. Werr L, et al. TERT Expression and Clinical Outcome in Pulmonary Carcinoids. J Clin Oncol. 2025;43:214–25.
67. Davis E, et al. Enhancer landscape of lung neuroendocrine tumors reveals regulatory and developmental signatures with potential theranostic implications. Proc Natl Acad Sci U S A. 2024;121:e2405001121.
68. Sen T, et al. Emerging advances in defining the molecular and therapeutic landscape of small-cell lung cancer. Nat Rev Clin Oncol. 2024;21:610–27.
69. Cooper AJ, et al. First Report of Response to Tarlatamab in a Patient With DLL3-Positive Pulmonary Carcinoid: Case Report. JTO Clin Res Rep. 2024;5:100750.
70. Caplin ME, et al. Lanreotide in metastatic enteropancreatic neuroendocrine tumors. N Engl J Med. 2014;371:224–33.
71. Rinke A, et al. Placebo-controlled, double-blind, prospective, randomized study on the effect of octreotide LAR in the control of tumor growth in patients with metastatic neuroendocrine midgut tumors: a report from the PROMID Study Group. J Clin Oncol. 2009;27:4656–63.
72. Kunz PL, et al. Randomized Study of Temozolomide or Temozolomide and Capecitabine in Patients With Advanced Pancreatic Neuroendocrine Tumors (ECOG-ACRIN E2211). J Clin Oncol. 2023;41:1359–69.
73. Walter T, et al. Oxaliplatin-Based Versus Alkylating Agent in Neuroendocrine Tumors According to the O6-Methylguanine-DNA Methyltransferase Status: A Randomized Phase II Study (MGMT-NET). J Clin Oncol. 2025;43:960–71.
74. Ayers M, et al. IFN-γ-related mRNA profile predicts clinical response to PD-1 blockade. J Clin Invest. 2017;127:2930–40.
75. Papaxoinis G, Lamarca A, Quinn AM, Mansoor W, Nonaka D. Clinical and pathologic characteristics of pulmonary carcinoid tumors in central and peripheral locations. Endocr Pathol. 2018;29:259–68.
76. Ura A, et al. Phenotypic Landscape of Pulmonary Neuroendocrine Tumors: Subtyped by OTP/ASCL1 Expression Correlated with Histology, Hormones and Outcome. Endocr Pathol. 2025;36:43.
77. Zuo W-L, et al. Ontogeny and biology of human small airway epithelial club cells. Am J Respir Crit Care Med. 2018;198:1375–88.
78. Allain EP, Rouleau M, Lévesque E, Guillemette C. Emerging roles for UDP-glucuronosyltransferases in drug resistance and cancer progression. Br J Cancer. 2020;122:1277–87.

Publisher's Note